

Helmholtz Cage Testing and Operating Determination Algorithm

Contributors: Evan Majd, Lindsay Taylor, Stephanie Wegner
University of Minnesota, Twin Cities

Attitude Determination and Control System, EXACT CubeSat Mission
Last Revised: May 08, 2017

This document is to be used to derive 2017 SmallSat Conference paper submission:
“Methodology for Software-in-the-Loop Testing of Low-Cost Attitude Determination Systems”

1.0 Abstract	2
2.0 Introduction	3
3.0 Apparatus	4
3.1 Pixhawk Flight Computer	4
3.2 Zero Gauss Chamber	5
3.3 Helmholtz Cage	6
4.0 Methods	8
4.1 Zero gauss chamber testing	8
4.2 Helmholtz cage testing	9
5.0 Results	11
5.1 Sensor Noise	11
5.2 Sensor Bias	11
5.3 Sensor Drift	12
5.4 Cross Axis Sensitivity	13
5.6 Error in Sensor Measurements	14
5.5 Error in Test Equipment	15
6.0 Applications to Determination Algorithm	16
6.1 Post-Processed Data with Matlab Algorithm	16
7.0 Conclusion	18
7.1 Testing & Analysis Conclusion	18
7.2 ADCS Year in Summary & Future Work	19
7.3 Important Afterthoughts & Unfinished Work	22
Appendix A - Testing Figures & Data Analysis	23
A1. Changing Magnetic Field with Constant Plate Orientation	23
A2. Plate Rotation in a Constant Magnetic Field	27
A3. Rotating Magnetic Field with Rotating Plate Tests	42
A4. Zero-Gauss Chamber Tests	46
A5. Gyroscope Noise and Drift Characterization	47
A6. Attitude Determination Algorithm Application	49
Appendix B - Atmel Development Board	56
Appendix C - Attitude Determination Algorithm Transfer from Matlab to C-Code	57
References	61
Acknowledgements	62

1.0 Abstract

Primary writer: Lindsay Taylor

Helmholtz cage testing was conducted to characterize low-cost gyroscope and magnetometer sensors for use in a CubeSat attitude determination and control system. Despite the attitude determination and control system being largely critical to mission success, testing documentation of attitude determination systems was found to be lacking after a survey of the appropriate published research. To address this shortcoming, a Pixhawk flight computer collected data in a Zero Gauss Chamber as well as a Helmholtz cage. The cage generated a three-axis magnetic field and had a three-axis rotating plate that could each be used to simulate readings that would be seen on-orbit. The gyroscopes and magnetometers were assessed by calculating their noise, bias, drift and error values. Data from the gyroscopes, magnetometers and accelerometers were used in post-processing through a written attitude determination algorithm. The overall goal of testing was to characterize a class of sensors with sparse documentation of necessary characteristics, and to determine whether low-cost sensors would be adequate for the attitude determination system accuracy required on the University of Minnesota's EXACT CubeSat mission.

After analyzing the data collected during testing, the Pixhawk gyroscopes had noise values of .0007 °/s, .0007 °/s and .0005 °/s in the X, Y, and Z axes, respectively. Drift in the gyroscope was calculated and reported, but found insignificant in terms of gyroscope performance. Error in gyroscopes was not able to be characterized as the true rate the plate was rotating at was unknown. The standard deviation in the gyroscope readings was found to be 0.1231°/s, 0.0955 °/s and 0.0879 °/s in the X, Y, and Z axes, respectively. These values were obtained from plate rotation through a constant on-orbit magnetic field about each axis.

The magnetometers were found to have noise values of .0020 milli-Gauss, 0.0004 mG and 0.0006 mG in the X, Y, and Z axes, respectively. The bias in the magnetometers were 0.0012 Gauss, 0.0055 G and 0.0034 G in the X, Y, and Z axes, respectively. Drift in the Z-axis was found to be 0.939 mG/sec, with negligible drift seen in the X and Y magnetometers. A longer testing period would be required to determine the reliability of these characterizations for drift. Magnetometer error varied greatly among the three testing days, but the more accurate values were assumed to be from the day when no magnetic field offsets were applied in the Helmholtz cage. The average magnetometer error was 2.19%, 1.06% and 3.99% for the X, Y, and Z axes respectively. Cross axis sensitivity was found in each axis, with the largest sensitivity being from the change seen in the X-axis while the Y-axis saw the true magnetic field change, dX/dY , with a value of 7.209%. The smallest sensitivity was found from the sensitivity of the X-axis while the Z-axis saw the true magnetic field change, dX/dZ , with a value of 1.362%.

The raw data taken by the Pixhawk's gyroscopes, magnetometers and accelerometers during tests in which the plate and magnetic field were rotating at the same time, about the same axis, were post-processed through the EKF. The X-axis rotation data was analyzed to compare the true attitude measured by the Pixhawk with a Vector Matching solution and EKF solution. After analyzing the post-processed data, the conclusion was that more testing and implementation of the sensor characteristics would be required to properly determine whether the low-cost sensors would be satisfactory in an on-orbit mission.

2.0 Introduction

Primary writer: Stephanie Wegner

Testing in a Helmholtz cage was conducted for the purpose of collecting data to characterize low-cost sensors and for post-processing use with an attitude determination algorithm. The attitude determination algorithm referenced in this paper is based in Matlab and uses the TRIAD algorithm with an Extended Kalman Filter. The TRIAD algorithm generates an initial attitude estimate from a direct cosine matrix relating data from the inertial and body reference frames as a vector to the sun. This gets fed into the EKF to propagate data and update the attitude estimate as accurately as possible. The testing data should be able to apply to other attitude determination algorithms, especially ones requiring the characterization of similar low-cost sensors. It is recommended the testing be repeated or continued once determination and control algorithms are implemented on a flight computer (or development board). In the case of this experiment, the algorithm used was not processing and solving its attitude in real time.

The Helmholtz cage used was located at the Honeywell facility in Plymouth, MN. The fixture set-up is described in Section 3.3. Over the course of three separate testing days, procedures were modified and improved to collect various data on a Pixhawk flight computer. The first day of testing consisted of utilizing the different features and testing abilities of the Helmholtz cage, by rotating a magnetic field and/or the plate about X/Y/Z axes. It was also used as a beta-test in order to learn the system to best plan future tests. The second day of testing was used to determine the proper step size to change the magnetic field rotation and plate rotation at the same rate. Data was also collected in a constant magnetic field while the plate was rotated. The final day of testing consisted of rotating the magnetic field and plate about the same axis at approximately the same time. Additionally, single-axis fields were generated to help characterize cross axis sensitivity of the magnetometers. Honeywell's Zero-Gauss Chamber, described in Section 3.2, was used on each testing day to collect data in a zero magnetic field environment.

The data collected was used to analyze sensor characteristics for the Pixhawk flight computer's magnetometers and gyroscopes. This included noise, bias, drift, cross axis sensitivity, and measurement error. Accelerometer data was used to verify validity of plate movements during testing using Earth's gravity field as a reference. The data from the magnetometers, gyroscopes, and accelerometers were also post-processed through the Matlab attitude determination algorithm to verify it could meet accuracy requirements of the system. This particular application is for a University of Minnesota CubeSat mission, where the satellite has a solar sensor that must be directed toward the Sun. It will use magnetorquers for control to change its attitude as needed. As seen in the diagram below, the determination algorithm reads data from magnetometers, gyroscopes, GPS, and sun sensors and combines this with magnetic field and solar ephemeris models to determine the satellite's change in attitude required.

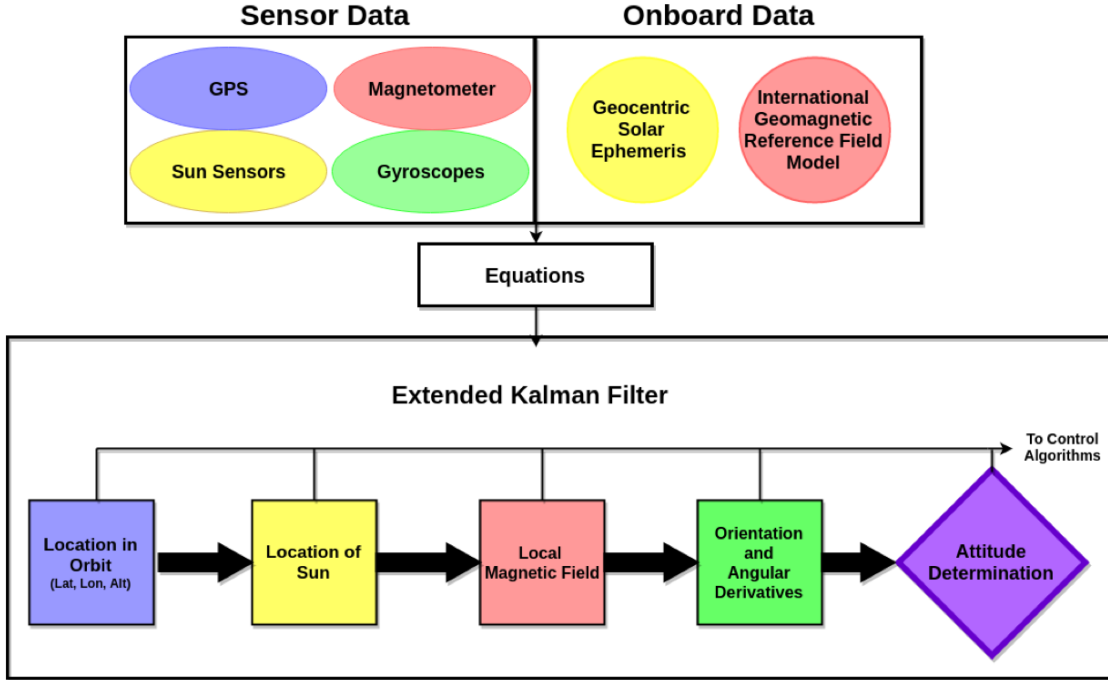


Figure 1: The structure of the attitude determination algorithm used in post-processing of testing follows this diagram. The data, shown at the top, corresponds with how it is used in the Extended Kalman Filter, shown at the bottom, by color coordination in the diagram. Overall, this shows how each element of the determination algorithm is connected, as well as what is required to determine the satellite's overall attitude.

The test performed that most closely resembled the satellite on orbit was when a magnetic field was rotated about an axis at the same time as the flight computer was rotated about the same axis. For the purposes of testing, the flight computer's measured acceleration (gravity vector) was emulated to be the “sun sensor” vector from the body to the sun for the algorithm. The gyroscope and magnetometer measurements were used as recorded during testing. Ideally, the analysis contained in this paper can be generally applied to a low-cost attitude determination system.

3.0 Apparatus

3.1 Pixhawk Flight Computer

Primary writer: Evan Majd

The Pixhawk was used to collect and characterize sensor data which was also fed into the MATLAB determination algorithm developed for a 3U CubeSat for post-processing. A Pixhawk is a 81.5 mm x 50.0 mm x 15.5 mm flight computer comprising of three important inertial sensors: accelerometers, magnetometers, and gyroscopes (each of these sensors being 3-axis capable). The gyroscopes, specifically the ST Micro L3GD20H 16 bit gyroscope, measure angular rates in three perpendicular axes. This is MEMS based with an I2C/SPI digital-output interface. The accelerometers

and magnetometers measure acceleration and magnetic field, respectively. They are specifically the one package ST Micro LSM303D 14 bit accelerometer/magnetometer and are also an I2C/SPI digital output interface. The magnetometer has a magnetic sensitivity of .08 mG/LSB and a magnetic cross axis sensitivity of +/- 1 %FS/Gauss. FS is the measurement range of the magnetometer in Gauss. By sensor fusion, the flight computer can also output true attitude which can be used for reference in a navigation algorithm. To output sensor measurements, QGroundControl software is used.

QGroundControl is a ground control software for MAVs and can be found at the following website: <http://qgroundcontrol.com/>. It was used as an interface and data logger to save each test as a text file, noting that specific sensors had to be selected to record and save data. The text files were converted to .mat files and were imported to Matlab for analysis. Physically, the Pixhawk was attached to a mounting plate and held in place by velcro during testing, as seen and described in Figure 5.



Image retrieved from https://3dr.com/wp-content/uploads/2017/03/Pixhawk_Top2.png

Figure 2: The Pixhawk is an advanced autopilot designed by the PX4 open-hardware project and manufactured by 3D Robotics. It features ST Microelectronics sensors and a NuttX real-time operating system. The micro USB to USB port is on the side of the device which was used for data logging and power supply. The white arrow indicates the positive X-direction (front), the Pixhawk's right side (appearing left in the picture) is the positive Y-direction, and the Pixhawk's down is the positive Z-direction. The Pixhawk's axes are defined in a "north-east-down" configuration.

3.2 Zero Gauss Chamber

Primary writer: Lindsay Taylor

A multi-layer Zero Gauss Chamber was used to determine magnetometer biases in the Pixhawk. The Zero Gauss Chamber is made from a soft magnetic alloy that works to cancel out any static or slow-changing magnetic fields, known as MuMETAL. Both a three-layer and five-layer chamber were used at the Honeywell facility for comparison of results. For most of the tests, the Zero Gauss Chamber was used for sensor calibration within the Helmholtz cage by matching the readings in the chamber to those seen in the Helmholtz cage when it was set at “zero” (known as the offsets set in the Helmholtz cage). Note that this methodology of calibration was later found to be flawed, as the offsets were really in the gyroscopes themselves, not the Helmholtz cage - if the plate was moved in the cage, the offsets did not move relative to the gyroscopes like they should have. The three layer Zero Gauss Chamber is pictured below:

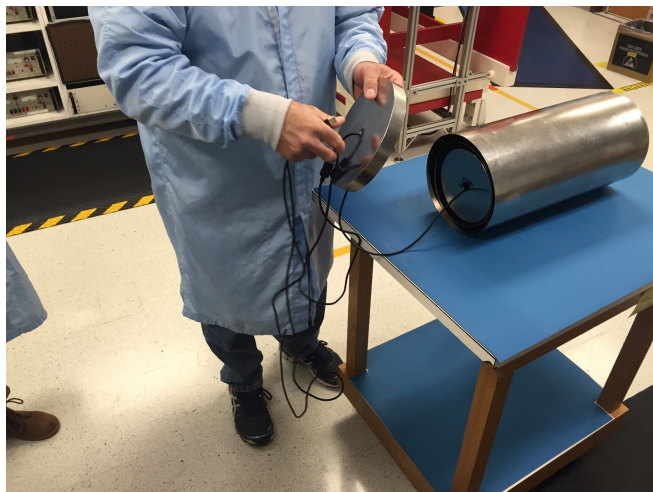


Figure 3: Setup of the three layer Zero Gauss Chamber for horizontal testing with the cap on. The Pixhawk flight computer is resting flat toward the back of the chamber for best results. Here, the USB cable is being drawn through the three cap lids.

3.3 Helmholtz Cage

Primary writer: Lindsay Taylor

For the testing described in this paper, the Helmholtz cage was used to characterize the Pixhawk sensors then post process data through the attitude determination algorithm. A Helmholtz cage is used to cancel out and create a three-axis uniform magnetic field that can closely replicate what a satellite would experience on-orbit¹. Many graduate level projects have focused on developing and building a Helmholtz cage, but in the interest of time and financial concerns, an industry testing lab was sought out.

Typically due to budget constraints, CubeSat hardware is rarely tested in a Helmholtz cage. Therefore, the Helmholtz cage’s data from this experiment should prove valuable for other collegiate

and low-cost small satellite missions. The three-axis Helmholtz cage that was used for testing is pictured below:

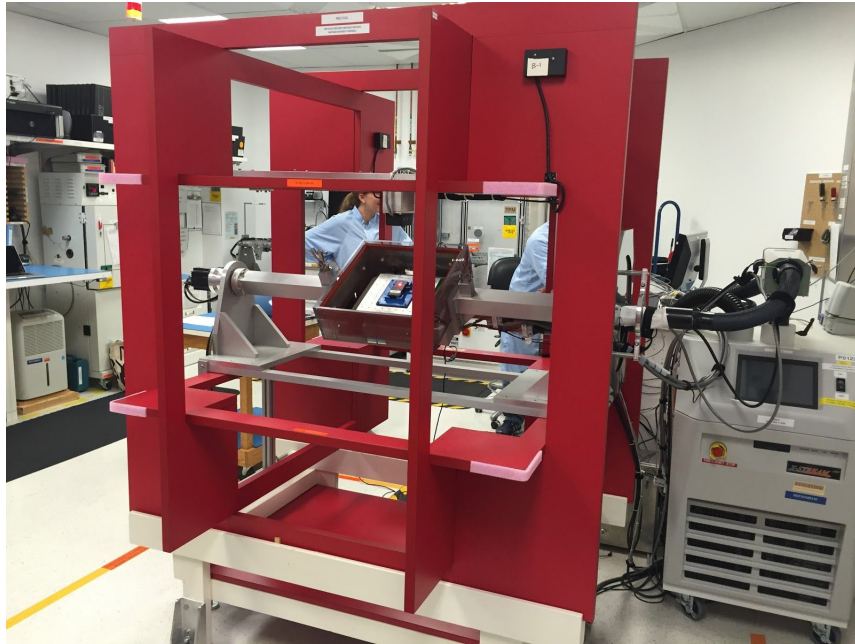


Figure 4: Helmholtz cage during plate rotation testing. The Helmholtz coils are in the red casing. The distance between the Pixhawk and the coils generates a more consistent magnetic field in the direct center of the Helmholtz cage (the most precise values are witnessed at the centerpoint). The magnetic field is generated by inputting the desired X, Y, and Z field values into the Helmholtz cage interface software, located on a computer (not pictured as it was located on the other side of the equipment).

A mounting plate was 3D printed with supports to center the Pixhawk in the middle of the coil's testing section as accurately as possible, in order to ensure a uniform magnetic field was seen on the flight computer. The mounting plate and integration inside the cage are pictured below:

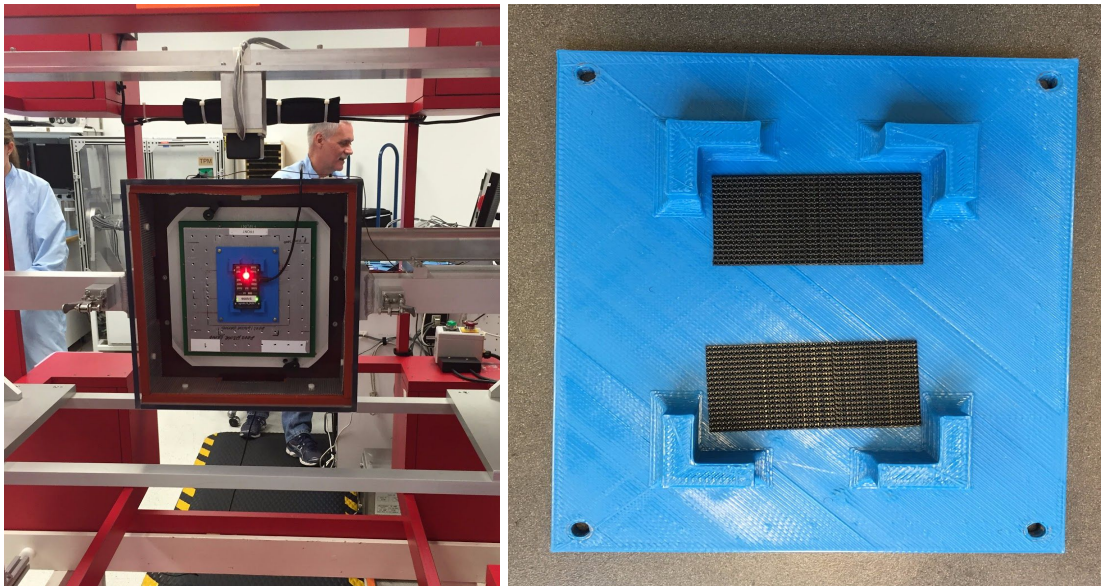


Figure 5: On the left side is the Pixhawk flight computer setup in the Helmholtz cage. This is an image of the Pixhawk during a rotation test (at -90°). On the right side is the 3D printed plate (blue) that the Pixhawk mounted to using Velcro. The mounting plate was bolted to the test area in the Helmholtz cage, and specifically printed with the bolt configuration sent to the team by Honeywell.

The axes of the Pixhawk and of the Helmholtz cage did not follow the same alignment. The Pixhawk used a “north-east-down” system while the Helmholtz cage followed the Right-Hand Rule. When the Y axes were pointing in the same direction, the X and Z axes would be pointing opposite for the Pixhawk and Helmholtz cage. A diagram was created to aid in visualizing the axes throughout the testing and data analysis:

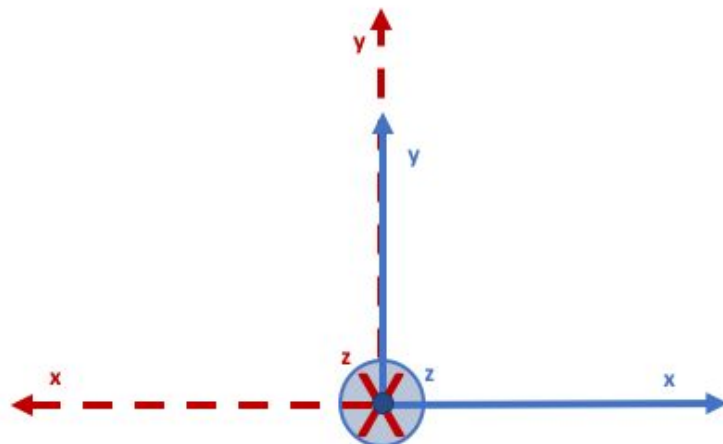


Figure 6: The axes alignment of the Helmholtz cage and the Pixhawk flight computer, as seen from a bird's eye view of the setup (see Figure 2 for better visualization of the orientation of the Pixhawk according to this photo). This diagram can be used as a reference to ensure consistent sign conventions. Blue represents the Helmholtz cage axes, while red represents

the Pixhawk flight computer axes. Note that the Z axis for the Pixhawk is INTO the page, while the Z axis for the Helmholtz cage is OUT of the page ($X_{\text{Pixhawk}} = -X_{\text{Helmholtz}}$, $Y_{\text{Pixhawk}} = +Y_{\text{Helmholtz}}$, $Z_{\text{Pixhawk}} = -Z_{\text{Helmholtz}}$). The diagram also helps to predict data that should be seen from the magnetometer readings based off the known magnetic field inputs in the Helmholtz cage.

4.0 Methods

4.1 Zero gauss chamber testing

Primary writer: Lindsay Taylor

The magnetic field experienced by the Pixhawk was measured using QGroundControl while in the Zero Gauss Chamber. Variation in the Pixhawk X, Y, and Z axes' magnetic field were used to calibrate the Helmholtz cage prior to testing. Gyroscope and magnetometer drift, noise, and biases were determined from the data collected. Since the initial purpose behind testing was to develop documentation on sensor characterization, it was found that these values would be important in describing the performance of our low-cost sensor choices.

Both a three and five layer Zero Gauss Chamber were used for this initial testing to see if any potential differences could be seen in the readings. Both chambers were tested lying horizontally, without a cap on, with the results seen in Figures 51 and 53. The three layer chamber was then tested with the cap on to see the lid's effect on the readings. The results are seen in Figure 52. Both biases (see Section 5.2) and drift (see Section 5.3) were calculated to determine sensor offsets and functionality. It was chosen to use data with the cap on to determine the offsets, as it was clear from the data trends seen in A4 that the most consistent results came from having the lid.

4.2 Helmholtz cage testing

Primary writer: Lindsay Taylor

Multiple tests were conducted in the Helmholtz cage to record data seen by the Pixhawk flight computer in various magnetic field and plate-rotational environments. Some tests were conducted in a constant magnetic field with the Pixhawk making rotations inside the test area. The Pixhawk sensor readings for these tests can be seen in Appendix A2. The constant magnetic fields tested include 0 mG on all axes (Figures 15-23), 250 mG on all axes (Figures 24-32), and a field that could be seen on orbit: $X = 226.44$ mG, $Y = -21.06$ mG, $Z = -117.39$ mG (all in the Helmholtz cage reference frame), a total magnitude of 255.93 mG (Figures 33-41). Other tests were done with a varying magnetic field, while the Pixhawk remained stationary. The sensor data recorded during these tests can be seen in Appendix A1. Lastly, in order to replicate a more realistic on-orbit environment, the Pixhawk and magnetic field were rotated at the same time about the same axis, during the tests seen in Appendix A3. It should be noted that there are slight variations in the data for this test since there was human lag time in starting both rotations. The two were unable to start rotating simultaneously leaving a slight time delay that can be seen in beginning of each test.

First Testing Day

Primary writer: Evan Majd

To test the static functionality of the Pixhawk's 3-axis magnetometers, the magnetic field of the Helmholtz cage was driven to the following values, consecutively, at a calculated rate of 10 mG/s: 0 mG, 250 mG, -250 mG, and 0 mG. This was run on all three axis. Next, a magnetic field with a magnitude of 250 mG was rotated about each axis at approximately 15 °/s. This rate was the average of the maximum gyroscope rotation readouts. These tests are in Appendix Figures E13-14.

To test the functionality of the Pixhawk 3-axis gyroscopes, the magnetic field of the Helmholtz cage was set to 0 mG while the mounting plate was rotated about the X-axis to the following values, respectively, at a rate of 22.5 °/s: 0°, 90°, 0°, -90°, and 0°. This rate was the average of the maximum gyroscope rotation readouts. This set of rotations was repeated for the Y and Z axes. After the magnetic field was set to 250 mG, the plate rotations were repeated in all three axes. The data from these tests can be seen in Figures 15-32.

Second Testing Day

Primary writer: Lindsay Taylor

In order to test the functionality of the magnetometers, gyroscopes, and accelerometers, the Pixhawk mounting plate was rotated through the Helmholtz cage with a stationary simulated "on-orbit" magnetic field being applied. The applied field was X = 226.44 mG, Y = -21.06 mG, Z = -117.39 mG with respect to the Helmholtz cage's frame of reference, at a total magnitude of 255.93 mG. Each Pixhawk axis was tested as the axis of rotation. For the X-axis rotation, the plate began at the Pixhawk reference frame of (-90°, 0°, -90°) and was rotated from -90° to +90° about the X-axis, then rotating back in the opposite direction to return to the initial position, as seen in Figures 33-41. To test the Y-axis, the plate began at (0°, -90°, 0°) and was rotated from -90° to +90°, returning to the initial position. The plate was oriented to (0°, 0°, -90°) then rotated about the Z-axis from -90° to +90°, returning to the initial position. The accelerometer readings were referenced (see Figures 34, 37 and 40) since it was known what results were expected during the rotations. Magnetometer, accelerometer, and gyroscope results were plotted for each axis' rotation, and can be seen in Figures 33-41.

Third Testing Day

Primary writer: Stephanie Wegner

The last day of testing had trials that were conducted in the Helmholtz cage as well as the Zero Gauss Chamber. The 3-layer Zero Gauss Chamber was placed both vertically and horizontally with the cap to collect data, as well as another extended period of time in its horizontal orientation to have better data to characterize magnetometer drift (see also in Section 4.1 above). The Pixhawk was screwed into the plate fixture in the Helmholtz cage and oriented in its initial position (X and Z axes in the Pixhawk reference frame pointing opposite of the X and Z axes in the Helmholtz cage, respectively. The Y-axis was pointing in the same direction in both the Pixhawk and Helmholtz frames. See Figure 6 if further clarification is needed.).

It was originally thought that in order to receive the most accurate test results, the bias seen in the Zero Gauss Chamber should be used to generate manual offsets in the Helmholtz cage that match what the sensors read in zero magnetic field. By mistake, the exact offsets were not recorded on this

day, however they can be estimated to be around the bias values seen in the Zero Gauss Chamber: 1.2 milli-Gauss in the X-axis, 5.5 mG in the Y-axis, and 3.4 mG in the Z-axis. It was discovered later that these offsets become an issue when the plate rotated, since the Pixhawk magnetometers that carry the bias would move relative to the fixed Helmholtz cage frame containing the offsets. The GUI on Honeywell's computer allowed for these manual offsets to be input outside the X/Y/Z axes for when a constant field would be generated. The offsets were not initiated during rotational magnetic field tests, so the constant magnetic field generation was the only test that was affected by the offsets this day. Since there were no plate rotations during this test, the data was easily able to be used during analysis.

In order to characterize magnetometer cross axis sensitivity, a constant magnetic field of was generated in one axis at a time. Each trial began with the magnetic field off, then one axis would be stepped up to 200, 225, 250, 275, or 300 milli-Gauss. After these five trials in the X-axis, the test was repeated in the Y-axis and Z-axis. Additionally for each axis, a trial was conducted going from 0 mG to 250 mG, down to -250 mG, and back up to 0 mG. Data extracted from some of these trials can be seen in Figures 7-12.

A magnetic field with a magnitude of 255.93 milli-Gauss was rotated 360 degrees about each axis (X/Y/Z) at a step size of 54 degrees in Honeywell's computer GUI for the Helmholtz cage. (Note the step size was specifically tested and chosen on the second testing day to rotate at approximately the same rate as the plate.) At the same time, the plate was rotated 180 degrees about the same axis in the same direction. Each trial was saved into separate files, and there were five trials on each axis. Honeywell's computer GUI did not allow for the plate rotation and magnetic field rotation to be started at the same time, so they were manually selected as quickly as possible after each other to ensure maximum overlap in rotation time. This did not affect the post-processing ability in the Matlab attitude determination algorithm, so the data collected was able to be used as intended.

5.0 Results

5.1 Sensor Noise

Primary writer: Evan Majd

The sensor noise was calculated by running a MATLAB script that records all the peaks and troughs of the signal noise, storing them in an array, and averaging them to get an amplitude. The outliers were taken out to ensure an accurate noise calculation.

The calculated magnetometer noise in the X, Y, and Z directions for the 3-layer Zero Gauss Chamber test were, respectively, .0018 mG, .0004 mG, and .0006 mG. The calculated magnetometer noise in the X, Y, and Z directions for the 5-layer Zero Gauss Chamber test were .0022 mG, .0004 mG, and .0006 mG. This gave an average magnetometer noise in the X, Y, and Z directions of .0020 mG, .0004 mG, and .0006 mG, respectively. This is small relative to the magnetic fields tested or seen on orbit, so they are likely not to significantly influence the accuracy of the magnetometers.

The calculated gyroscope noise in the X, Y, and Z directions for the 3-layer Zero Gauss Chamber test were, respectively, .0007 °/s, .0006 °/s, and .0005 °/s. The calculated gyroscope noise in the X, Y, and Z directions for the 5-layer Zero Gauss Chamber test were .0007 °/s, .0007 °/s, and

.0005 °/s. This gave an average gyroscope noise in the X, Y, and Z directions of .0007 °/s, .0007 °/s, and .0005 °/s, respectively. This is minimal relative to the accuracy requirements of the attitude determination system, and would not have a significant impact on the gyroscope performance.

5.2 Sensor Bias

Primary writer: Lindsay Taylor

The magnetometer readings were taken from the Pixhawk while in Zero Gauss Chamber testing to characterize the inherent sensor bias. Four test setups were conducted to see if this would cause any major difference in sensor readings. In the test where the three-layer Zero Gauss Chamber was lying horizontally without a cap on (Figure 51), a bias was seen for the X, Y, and Z axes of 0.0012 G, .0058 G, and 0.0055 G, respectively. In the same chamber lying horizontally but with a cap on, a bias was seen for X, Y, and Z of 0.0012 G, 0.0055 G, and 0.0034 G, respectively. The final test in the three-layer chamber was by standing it vertically with the cap on (Figure 52). A bias was seen in the X, Y, and Z axes of 0.0021 G, 0.0057 G, and 0.0101 G, respectively. These biases are small relative to the expected magnetic field values to be seen on orbit, but important to note for sensor accuracy comparisons.

The five-layer Zero Gauss Chamber was tested, mainly to see if there was a difference in data in a chamber with added layers. This chamber was tested lying horizontally without a cap on (Figure 53). The bias seen in the X, Y, and Z axes were 0.0022 G, 0.0052 G, and 0.0062 G. The bias was comparable to the three-layer Zero Gauss Chamber, showing the amount of layers required to cancel outside magnetic field was enough at three. It was found that the three and five layer Zero Gauss Chambers do not demonstrate any superior performance over the other in sensor biases. The biases show a detectable, though still not significant, variation between the cap being on or off. If future testing were to be conducted, the chamber with a cap would be utilized since the slight difference was found.

The consistency in the Zero Gauss Chamber biases was compared to biases in the Helmholtz cage. Biases were calculated using tests where the initial magnetic field was starting at (0, 0, 0) G, to see any offset each axis would have in zero magnetic field. Tests from two separate days were analyzed for comparison, as the first day's tests had no offsets set in the Helmholtz cage while the third day's tests did. The first day's tests used were when the magnetic field was swept in each axis from 0 to 250 mG, then down to 250 mG and back to 0 - the data used for bias being from before the sweep occurred (so when the axis was starting at 0 mG). The second day's tests used were when the magnetic field was set as a constant in one axis - the data used for bias being from before any magnetic field was entered. From the first day's tests, an average bias was seen in X, Y, and Z of -0.0018 G, 0.0033 G, and 0.0079 G, respectively. From the third day's tests, an average bias was seen in X, Y, and Z of -0.0015 G, -0.0104 G, and 0.0079 G, respectively. The Y axis bias was the only one that was significantly different between the two days of testing, so it is possible that the Helmholtz cage offsets had influence on the magnetometers' readings in zero magnetic field. The magnetic field biases were again small relative to expected magnetic field values on orbit, but were used in the comparisons for magnetometer sensor accuracy.

5.3 Sensor Drift

Primary writer: Lindsay Taylor

Sensor drift was observed and analyzed for the magnetometers and for gyroscopes. Drift was seen primarily in the Z-axis magnetometers, and more significantly without the Zero Gauss Chamber lid closing the test area. The tests without the cap are seen in Figures 51 and 53. The average magnetometer drift for the Z-axis without the cap on was found to be 2.11 mG/sec. This test was compared to drift calculations with the cap on, as seen in Figure 52. The average magnetometer drift for the Z-axis with the cap on was found to be 0.939 mG/sec.

It is interesting to see the Z-axis magnetometer significantly displaying more drift than the X or Y-axis magnetometers. It is possible that the cause of the drift seen is temperature related. The Pixhawk magnetometer has a magnetic sensitivity in relation to temperature of $\pm 0.05\text{ \%}/^{\circ}\text{C}$. Since no temperature changes were happening in the Zero Gauss Chamber, it is assumed that any temperature changes would have been caused by the flight computer self-heating. Ultimately, it may be an anomaly in the data as to why the dramatic drift is seen specifically in the Z-axis while testing in the Zero Gauss Chamber. This amount of drift was not seen when the magnetometers were being tested later in the Helmholtz cage. It was researched and determined that drift measurements should take place over more time than what was allotted in these tests. For future testing, it would be important to include a longer test interval in the Zero Gauss Chamber to accurately observe sensor drift behavior.

Gyroscope drift was calculated from Figures 54 and 55 and is reported within their captions. The gyroscope drift witnessed during testing was insignificant and highly unlikely to affect gyroscope performance.

5.4 Cross Axis Sensitivity

Primary writer: Stephanie Wegner

Cross axis sensitivity can be observed in the magnetometer sensor data, specifically in Figures 7 through 12. This type of error occurs when there are changes in measurement picked up on axes other than the one aligned to the generated field in the Helmholtz cage. In other words, the actual magnetic field is aligned differently than what the sensors observe, causing some interference in some axes relative to others. The testing that was used specifically for this analysis generated a constant field in the Helmholtz cage in one axis at a time. The changes in each axis were recorded as multiple trials collected data from fields generated between 200 milli-Gauss and 300 milli-Gauss (specifically containing data for jumps from 0 to 200, 225, 250, 275, and 300 mG).

The data shows that the general trend for cross axis sensitivity is constant across the varying magnetic field inputs. When the fields were generated in the X-direction, the Y-X axis sensitivity, dY/dX , measured to be an average of about 1.759% with a standard deviation of 0.359%. The Z-X axis sensitivity, dZ/dX , was an average of 2.780% with a standard deviation of 0.329%. The five field trials generated Y-direction showed the X-Y axis sensitivity, dX/dY , to be an average of 7.209% with a standard deviation of 0.641%. The Z-Y axis sensitivity, dZ/dY , was an average of -1.523% with a standard deviation of 0.369%. The fields were then generated in the Z-direction, where the X-Z

sensitivity (dX/dZ) was an average of 1.362% with a standard deviation of 2.486%, and the Y-Z sensitivity (dY/dZ) was an average of -1.545% with a standard deviation of 0.728%.

The standard deviations were all very low given the sample sizes of five trials, except for the characterization of the X axis in the Z-axis generated fields. Perhaps more data would need to be collected to better characterize the cross axis sensitivity for magnetic fields generated in the Z-axis given its higher standard deviation. The largest average cross axis sensitivity was seen for dX/dY , which was about four times as large as that seen for dY/dX . It is also interesting to note that the dZ/dY and dY/dZ cross axis were both negative, and nearly the same at -1.5%. Overall, cross axis sensitivity was able to be characterized as a percentage of the reading seen in the sensitive axis. Further testing could be done to more accurately represent the cross axis sensitivity by repeating the same trials, or testing in a wider range of generated magnetic fields.

5.6 Error in Sensor Measurements

Magnetometers

Primary writer: Stephanie Wegner

Error in magnetometers can be characterized by comparing the magnetic field that was input into the Helmholtz cage to the data taken from the Pixhawk's magnetometer. Data from the first day of testing, as seen in Figures 13 and 14, as well as the third day of testing, represented by Figures 7-12, were analyzed at points in which the Helmholtz cage magnetic field input was known and not at zero. The error was calculated by taking the difference between the actual field (assuming negligible error in the Helmholtz cage) and the magnetometer reading, then dividing by the actual field.

There was a noticeable difference in the average error for the different days of testing due to the small offsets put in the Helmholtz cage on the third test day (see Section 4.2 for further clarification). The X-axis error was the exception, as the average error on the analyzed data from the first testing day was 2.19% while the average error was 3.19% for the third testing day. With both days' data combined together, the overall average X-axis error was 2.73% with a standard deviation of 1.22%. The Y-axis saw more of a difference between the two testing days, where the first testing day without offsets saw an average of 1.06% error with a standard deviation of 0.87%. The third day's magnetometer readings in the Y-axis had 5.75% error with a standard deviation of 2.15%. The most error in any axis occurred in the Z-axis readings from the third day of testing, where there were offsets set in the Helmholtz cage. The mean error for this day was 11.03% with a standard deviation of 4.37%, which can be compared to a mean error of 3.99% with a standard deviation of 2.12% from the first day's Z-axis magnetometer readings.

Such a large difference in both the mean and standard deviation for the Z-axis readings between the two testing days is interesting when compared to the similarity in the X-axis readings. When looking at the estimated offsets that were put in the Helmholtz cage, one can see that the Y-axis actually had the largest offset, with the Z-axis being second, and the X-axis being smallest. The trend between the X and Z axes match that of the error difference, but the Y-axis does not have a larger error as might be expected if the error was directly correlated to the third day's axial magnetic field offset. More experimental trials could be conducted to ensure more statistically valid testing data, in order to help to determine the error in each axis and overall error trends more confidently.

Gyroscopes

Primary writers: Evan Majd and Lindsay Taylor

The standard deviation from gyroscope readings was calculated for the X, Y, and Z axes, as the error itself could not be calculated due to a lack of knowledge on the actual plate rotation rates. Data from rotating the Pixhawk plate through a constant on-orbit magnetic field value was used to determine this error. Figures 35, 38, and 41 show the gyroscope readings from one trial being analyzed (for X, Y, and Z respectively). Nine trials were taken for each axis with the standard deviation of the raw data being calculated for each axis.

The standard deviation totals were found to be 0.1231 deg/s, 0.0955 deg/s, and 0.0879 deg/s for the X-axis gyroscope, Y-axis gyroscope, and Z-axis gyroscope, respectively. It should be noted that variations from zero are seen in the gyroscopes that are not being rotated, similar to how the cross-axis sensitivity was observed in the magnetometers. Looking at the scale on the Y-axis (Figures 35, 38 and 41), the variations remain less than 1 deg/s. Potential reasons for these slight fluctuations could come from gyroscope misalignment inside the Pixhawk, alignment of the Pixhawk on the plate as it sat on velcro, or slight vibrations during testing.

5.5 Error in Test Equipment

Helmholtz Cage

Primary writer: Lindsay Taylor

Helmholtz cage error could have been caused by two main factors, the first being the plate's placement inside of the coils. It would be desireable to have the magnetometers in the Pixhawk flight computer located at the centerpoint of the cage, as it is known that the most precise magnetic field values would occur at this point. Since the 3D mounting plate and the Pixhawk could not be perfectly square inside the cage due to shape constraints, it is possible that this may have been the cause for some of the observed data variations.

The second factor comes from inherent error present in the Helmholtz cage. Honeywell provided their Helmholtz cage characterization data and reported that with forced magnetic fields up to approximately 50,000 nT (500 mG), error was measured to be less than 30 nT (0.3 mG). This range encompasses all tests performed in the Helmholtz cage for the purpose of this system. It is reasonable to assert that deviations in data collected from the Helmholtz cage could be caused by this inherent error.

Pixhawk Flight Computer

Primary writer: Stephanie Wegner

The Pixhawk flight computer could have generated some error in readings, primarily due to sensor positioning within the manufactured case. If the magnetometer was not exactly in the center of the Pixhawk, the Helmholtz cage's generated field would have been read in a slightly off-centered position. Additionally, the velcro mounting of the flight computer on the 3-D printed plate could have created more variance in its mounted orientation than if it was sitting flat on the a rigid plate. If the magnetometers and gyroscopes were not oriented exactly perpendicular in their three axes, some error would be seen in the measurements. However, this should have also been characterized in its bias and cross axis sensitivity. Part of using a low-cost system means less accuracy and precision in

the flight computer's hardware. Although error generated from the Pixhawk and other low cost systems can affect their measurements, the goal is that the error is not great enough to exceed the accuracy requirements of the system itself.

6.0 Applications to Determination Algorithm

6.1 Post-Processed Data with Matlab Algorithm

TRIAD Algorithm

Primary writer: Evan Majd

The TRIAD algorithm is one of the earliest and simplest solutions to spacecraft attitude determination. Given the knowledge of two vectors, one vector of the satellite in the body frame, and one of the satellite in the reference frame, a direct cosine matrix can be found relating the two coordinate frames. To create the direct cosine matrix, R_i^b , 6 vectors need to be calculated:

$$t_{1b} = s_b \quad (1)$$

$$t_{2b} = \frac{s_b \times m_b}{|s_b \times m_b|} \quad (2)$$

$$t_{3b} = t_{1b} \times t_{2b} \quad (3)$$

$$t_{1i} = s_i \quad (4)$$

$$t_{2i} = \frac{s_i \times m_i}{|s_i \times m_i|} \quad (5)$$

$$t_{3i} = t_{1i} \times t_{2i} \quad (6)$$

These vectors are used to create the rotation matrix from inertial vector to the sun to the body vector to the sun, which is then used as the initial attitude estimate for the EKF algorithm.

$$R_i^b = [t_{1b} \ t_{2b} \ t_{3b}] [t_{1i} \ t_{2i} \ t_{3i}]^T \quad (7)$$

The vectors used in the Matlab algorithm are the sun vectors in the body and inertial frames, s_b and s_i , and the magnetic field vectors in the body and inertial frames, m_b and m_i , respectively. The sun vector in the body frame, s_b , would be output sun sensor vector measurements. The magnetic field vector in the body frame, m_b , would be the output normalized magnetometer measurements. The sun

vector in the inertial frame, s_i , is the sun vector found from the Solar Ephemeris Model (a blockset function in Matlab). The magnetic field vector in the inertial frame, m_i , is the normalized magnetic field vector from the International Geomagnetic Reference Field Model (another blockset function in Matlab).

For post-processing, it is important to note that the sensors intended for use in the TRIAD algorithm were not the same as those taken and used from testing data. The sun sensor vector in the inertial frame, s_i , was simulated by using Earth's Gravity vector, or a unit vector pointing in the negative Z-direction in the inertial frame, [0 0 -1]. The sun sensor vector in the body frame, s_b , was simulated to be the output accelerometer sensor measurements. Therefore, the simulated "sun" was always pointing toward the center of the Earth during all tests.

EKF Algorithm

Primary writer: Evan Majd

The Extended Kalman Filter (EKF) is a nonlinear form of the Kalman Filter which linearizes about an estimate of the current mean and covariance of the satellite attitude. It can give reasonable performance, and is the standard in space-based navigation systems. The Extended Kalman Filter in the attitude determination system to be used for the EXACT CubeSat mission takes in the gyroscope vector, the sun and magnetic field vector in the body frame, the sun and magnetic field vector in the inertial frame, the previous quaternion estimate, and the previous state error covariance. It outputs the attitude quaternion estimate of the satellite, the state error covariance, and the attitude error computed from the Kalman gain.

Post-Processing Analysis

Primary writer: Stephanie Wegner

Post-processing was performed to figure out the accuracy of the Matlab attitude determination system given the Pixhawk sensor characteristics. The tests used in the post-processing were those that rotated magnetic fields about the same axis as a plate rotation. The testing data can be found in Figures 42-50, in Appendix A3. The data for each rotation test was loaded into a code modified to drive the Extended Kalman Filter, using the gyroscope data, magnetometer data, and accelerometer data from the Pixhawk with an initialized inertial sun vector and inertial magnetic field vector called in the beginning of the driver. For the purposes of space and length of this paper, the code used to drive the EKF, and the EKF code used can be found in the linked folder: [\[LINK\]](#). It should be noted that when the data was being processed, the vector matching solution was used as the measurement update, so the EKF was likely estimating the attitude by a balance between the vector matching solution and the true attitude. To test this hypothesis, the measurement noise was inflated (the measurement noise is represented by matrices R_s and R_m on lines 77 and 79 in EKF_edited4.m). It was observed that changing the sun sensor measurement noise, R_s , did not affect the resulting EKF attitude estimation as much as inflating the magnetometer measurement noise, R_m . The noise value that ended up providing an EKF estimation closest to the true attitude of the Pixhawk was 0.7. This is compared to the value that it had originally started with in the EKF algorithm was 0.05. Normally it is poor practice to "tune" or change these measurement noise values at random, but for the purposes of this experiment, it was used as a troubleshooting method to find and attain the most accurate EKF estimation possible.

The post-processed data for the X-axis rotations (five trials total) can be seen in Appendix A7. The difference in the EKF estimation can be seen in each figure between the magnetometer measurement noise values of 0.05 and 0.7, showing that the 0.7 noise value generates significantly less error. The euler angle estimations between the true attitude, vector matching solution, and EKF estimated attitude are all shown in figures to visually see the difference in actual attitude and the estimations. Then, the errors between the EKF and true attitude were plotted to see its variation over time. The bias for each axis was also plotted over time, as the EKF continuously updated the bias estimate. The Y and Z axis rotations were processed and plotted (and saved in this folder: [\[LINK\]](#)), but are not included in this report and should be analyzed in the future in order to fully understand the limitations of the attitude determination algorithm with the Pixhawk sensor accuracy. It seems that the error in the yaw measurements should be looked at closer as they were the highest around 20 degrees, whereas the pitch and roll EKF estimates were typically within 4 degrees of accuracy from the true attitudes. Overall, the system should be analyzed more before making any final conclusions on whether the Pixhawk sensors are accurate enough to be used in orbital attitude determination applications.

7.0 Conclusion

Primary writer: Stephanie Wegner

7.1 Testing & Analysis Conclusion

The purpose of the extensive testing and analysis of the Pixhawk's magnetometers, gyroscopes, and accelerometers was to characterize whether the sensors used would be sufficient and accurate enough to use for an on-orbit attitude determination system. After surveying relevant literature on CubeSat attitude determination systems, the team realized that there is hardly any testing documentation on attitude determination systems that use low-cost sensors. The purpose of testing the Pixhawk became to not only test the functionality of a written attitude determination algorithm, but also to find out whether conclusions could be made about sensor reliability and accuracy for low-cost attitude determination systems in general.

Using the data collected from testing, the gyroscopes and magnetometers were characterized. The average noise seen in the magnetometers were .0020 mG, .0004 mG, and .0006 mG, respectively in the X, Y, and Z directions. The average noise observed in the gyroscopes were .0007 °/s, .0007 °/s, and .0005 °/s, again respectively in the X, Y, and Z directions. Bias in the magnetometers were also characterized, which varied slightly during different tests and can be seen further in Section 5.2. Magnetometer sensor drift was observed to be 2.11 mG/sec in the Z-axis when tested in a Zero Gauss Chamber without the cap on, and was 0.939 mG/sec with the cap on. The difference seen between the two can be seen in Figure 52, but it is recommended that to get a more accurate prediction for sensor bias that it should be tested longer to collect more data over a longer period of time.

Cross axis sensitivity was characterized for each axis of the magnetometer, measured by the change in magnetic field seen in an axis it wasn't supposed to over the change in magnetic field of the axis that was supposed to be seeing a change in magnetic field. The results of the cross axis

sensitivity analysis can be seen in Section 5.4. Lastly, the error in sensor measurements and equipment were discussed. Due to difference in testing methods on different days, it was difficult to characterize the error in magnetometer measurements fully. However, it is estimated that the more accurate representation of the error would be from the first testing day (the day without any magnetic field offsets entered in the Helmholtz cage), where the average X-axis error was 2.19%, the average Y-axis error was 1.06% , and the average Z-axis error was 3.99%. While the overall error of the gyroscope could not be calculated, the deviation between tests that should have seen the same results were compared. The standard deviation totals were found to be 0.1231 deg/s, 0.0955 deg/s, and 0.0879 deg/s for the x-gyroscope, y-gyroscope, and z-gyroscope, respectively. The error in the Helmholtz cage and Pixhawk flight computer (including physical mounting system inside the cage), were considered and likely had a minor impact on measurements taken during the testing procedures.

Data from plate and field rotations about the same axis at the same time were used in post-processing to test the attitude determination algorithm and its accuracy. The rotations about the X-axis were used while the noise values within the Extended Kalman Filter were inflated to see if the accuracy of the algorithm would change for different predicted noise values in the sensors. The algorithm tested and preliminary analysis of results are described in further detail in Section 6.1, and it is recommended to conduct further analysis in the future to see if the Y and Z axes show different trends. From the data that was analyzed, given the yaw-axis error is irrelevant as its plane faces the sun, the pitch and roll axes are within reasonable error that the Pixhawk sensors could be used reliably enough in an on-orbit determination system to face the sun. This, however, would be difficult when trying to control the spacecraft, as its accurate orientation would need to be known to command proper torques.

Various sensor characteristics were analyzed following testing of the Pixhawk flight computer in a Helmholtz cage, allowing post-processing of the data through an attitude determination algorithm. For all tests conducted, the data was analyzed to the extent that was observable in its trends and meaning with what it should have seen. The post-processing with the attitude determination algorithm is in its preliminary stages, however the data is ready to be analyzed for overall determination system conclusions to be made. For now, the best conclusion is that further testing and analysis, on both the sensor reliability and the algorithm's performance, should be conducted before saying that low-cost sensors are able to be used accurately enough on an on-orbit determination system.

7.2 ADCS Year in Summary & Future Work

Between the Fall 2016 and Spring 2017 semesters, there was much progress for the Attitude Determination and Control System for the University of Minnesota's EXACT CubeSat mission. The Fall 2016 semester can be referenced in depth through the end-of-semester documentation and Critical Design Review of the system [\[LINK to folder\]](#). At the conclusion of that semester, the attitude determination algorithm was near completion in Matlab, with the TRIAD algorithm functioning properly and a few bugs to work out before finalizing the Extended Kalman Filter code. The control algorithm was a bit further behind as the students working on it were concurrently enrolled in their first classical controls course and there was a learning curve to designing a controller, let alone a controller for this specific application and evolving design. The preliminary and changing characteristics of the CubeSat itself showed that the work done on the control algorithm could only go so far without accurate or close

to finalized mass properties of the system; otherwise the work tuning the controller would just have to be re-completed again later. The navigational system and detumbling algorithm for the satellite were also preliminarily designed, but should be looked at in further detail once the determination and control algorithms are more ready to be integrated to work together. Lastly during fall semester, there was research conducted for similar previous work in order to find the best way to test an ADCS or small satellite. The work done in researching and planning for testing continued to develop as the team analyzed the best way to approach the build and test of the ADCS system, particularly given the time constraints of one semester to do so for the senior design course.

One of the first issues that arose for testing was the lack of knowledge and research for the sun sensor implementation. Finding the proper sun sensor for the project and determining how to test it would take more time than could be allocated to do so. It was decided that the sun sensor data would be simulated for the semester. The control algorithm was also much further behind in development than the determination algorithm, and given that the team downsized from eight people to four, there would not be enough people to work on both of these at the same time to keep up with the design and build requirements of the semester. Since the determination algorithm was further along in development and closer to being ready to test on a physical level, it was decided the determination algorithm would be the focus for the semester. Next, the issue became what physical system that should be used for the build and test. The University's CubeSat team was working on a development board for the Atmel flight computer that has been chosen to fly on the mission. The team received all information for the build and operation of the flight computer to that point, and it was concerning that there would be a lot of development and debugging that would have to take place in order to even communicate to sensors yet. Not only did our system build and test for the semester require the collection of data from sensors such as magnetometers and gyroscopes, but the development board also operated under a Real Time Operating System (RTOS), which would take more time to figure out than the team could afford to use. While the team was still interested in learning about the development board and begin progress on its build, it was decided that a more simple but similar flight computer should be used for the testing of the attitude determination algorithm. The Atmel development board is based on coding in C, which the Pixhawk flight computer also had in common. Professor Gebre had previous experience in programming a Pixhawk, and the Aerospace Engineering & Mechanics department had the hardware readily available to borrow.

While the original plan was to purchase and develop the Atmel development board in parallel with using the Pixhawk to test the determination algorithm, the focus became fully toward the determination algorithm and planning for testing. The Pixhawk was extremely convenient to use given it came with all sensors required for testing the determination algorithm, and because it came with a somewhat user-friendly software interface. Although an accelerometer is not technically used in the determination algorithm, it was able to be utilized during testing as Earth's gravity was used as a simulated vector pointing at the sun (the accelerometer data was used as sun sensor data in the post processing of the data with the algorithm). There were some challenges that came from converting the determination algorithm from Matlab to C-code, especially learning the Pixhawk libraries and syntax to use. The team continued to plan converting the whole code to implement on the Pixhawk and run during at least one testing day.

Planning for testing consisted of communication with Honeywell for questions on their equipment and scheduling three days of testing. The team was planning for the first day to take a long

and for something to go wrong enough that could be corrected for future tests. Aluminum was going to be used as a mounting plate for the least amount of magnetic interference, but a 3D printed plate was chosen instead to ensure the Pixhawk could be mounted in the exact center of the plate. Honeywell sent the bolt pattern for mounting the plate on the fixture, which was able to be implemented into the design and print of the plate itself. The first day of testing only took two hours, as the setting up of the plate on the Helmholtz cage fixture took about 15 minutes, and tests were able to be run to collect data using all of its available features (including plate rotations, magnetic field rotations, and constant magnetic field implementation). The Pixhawk was also set into the Zero Gauss Chamber to see what data might look like in a zero magnetic field environment.

Moving beyond the first testing day, plans were developed that could test the attitude determination system. It was advised that the most realistic testing scenario that could be close to what would be seen on the CubeSat in orbit was a plate rotation with a magnetic field rotation occurring at the same time in the same direction. The second test day was used to determine the rotation rate of the magnetic field that would match the rotation of the plate, as it was not known or recorded directly in Honeywell's previous experience. Data with plate rotations were also collected to use for characterization of sensors. The determination algorithm conversion to C-code was not complete by the third testing day so the rotation data was collected to use for post-processing with the Matlab determination algorithm, in addition to collecting constant magnetic field data for sensor characterization. At that point, the determination code conversion was stopped to work on testing analysis and the final documentation for the semester. The code conversion and where it was stopped are described further in Appendix C.

The testing data contained in this paper and concluded in Section 7.1 above should be applicable for the future of the CubeSat project, specifically for the EXACT mission. The sensors from the Pixhawk are on the same level of cost and accuracy to the sensors being used with the Atmel, so the characteristics found through testing may be able to be applied in the algorithms and predictions during flight. Additionally, the exploration of post-processing can set a path for using testing data retroactively to test the accuracy of the final determination system. There can also be improvements made if future tests are conducted on the Attitude Determination and Control System. One important mistake that could be learned from is to not change any of the Helmholtz cage offsets just from the bias seen in a Zero Gauss Chamber. If plate rotations are being conducted, the offsets that should be contained in the flight computer's frame of reference still remains in the Helmholtz cage's frame of reference and can greatly impact the data and analysis. There can also be more work done to plan and test the simultaneous plate and magnetic field rotation, as the end results did not seem accurate toward what was expected.

Other future work for the Attitude Determination and Control System, aside from building off the testing experiences from this semester, can be prioritized according to the project's timeline. The parts of the system that are currently most behind appear to be the sun sensor integration and attitude control algorithm. After the control algorithm is complete in Matlab, it will be important to start integrating it with the determination algorithm and figuring out how they will work together, and with the flight computer. The detumbling algorithm should be implemented at this time as well. Once all code is converted to C (also not a trivial task that will take time), the ADCS can be implemented onto the Atmel flight computer. At this point, testing with the entire system is highly recommended, potentially using the same Helmholtz cage setup that was used this past semester. Throughout the process of creating

and implementing the ADCS, it will be important to assess risks posed to the the system and potential failure modes to be mitigated. A potential risk mitigation worth looking into would be a magnetometer-only determination algorithm that does not depend on sun sensor data to determine attitude. The testing should also help to some of the issues that could arise during flight and verify if the control system can work to output torque according to its maneuver to point toward the simulated sun. Overall, there is much work to be done on the Attitude Determination and Control System, but this year's work provides a foundation and vision for the future of the system.

7.3 Important Afterthoughts & Unfinished Work

- Extended drift testing time - typically drift is reported as magnitude/minute, and we only had sufficient data for magnitude/second. This could possibly explain the extensive drift seen in the z-magnetometer, although we were unable to come to a sound conclusion on this. We would recommend conducting the Zero Gauss Chamber test again for a more extended period of time (at least longer than 5 minutes).
- Should work on characterizing gyroscope bias (no current work done for this) - could potentially be used to help analyze attitude determination algorithm performance
- Drift was characterized in gyroscopes by looking at testing data from Helmholtz cage when plate was not rotation (e.g. only magnetic field was changing during tests) - see Figures 54-55. If there is not enough data to work with currently, could test this by collecting long data set (longer than 5 minutes?) in the Helmholtz cage without rotating the plate. Could try with and without magnetic fields to see if there is any magnetic interference with gyroscope as well.
- Rotation testing data characterization (see Appendix A3) - wasn't able to figure out if the plate and magnetic field were rotating about the appropriate axis at the same time and/or same direction. After looking at the magnetometer data some questions came to mind. Was the magnetic field rotating about the X-axis clockwise while the plate rotated counterclockwise, or were they both rotating clockwise? Also, was the plate actually moving 180 degrees about the X-axis while the magnetic field rotated 360 degrees, or were they both rotating the same amount? Did the magnetic field and plate end their motion at the same time during testing? (NOTE: during testing day, the rotation and magnetic field changes would appear to end at approximately the same time, depending how close together in time their rotations were initiated.)
- Post-processing rotation-test data with EKF - for each X/Y/Z axes, some of the tests would attempt to be plotted through the EKF driver and would not plot EKF solution (see Appendix A7, Trial 2). Unexpected to see this issue because in the raw plotted rotation test data (see here: [\[LINK\]](#)) there are not anomalies (at least none we found) between trials that prove why EKF solution wouldn't plot for certain trials.
- Uncertain if analysis of post-processed data is correct in figure descriptions that show bias (Figures 58, 61, 64, 67). Overall lack of understanding about what the bias trends mean - analysis of bias is lacking in paper, so implications toward results were not made.

Appendix A - Testing Figures & Data Analysis

A1. Changing Magnetic Field with Constant Plate Orientation

Single Axis Field Test

Primary writer: Stephanie Wegner

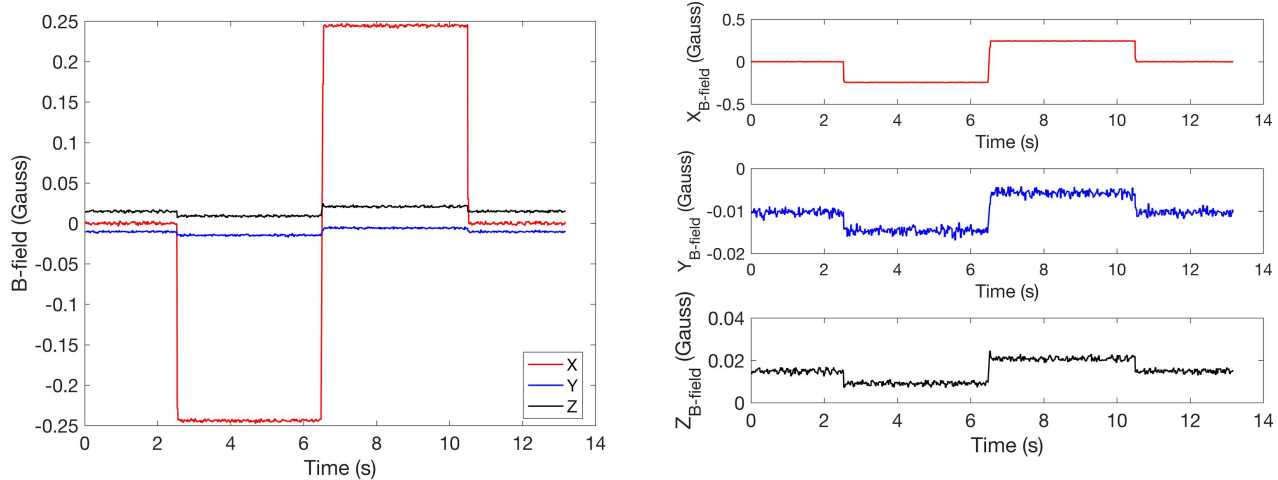


Figure 7: The magnetic field was set at zero, then set at 250 mG in the Helmholtz cage X-axis, down to -250 mG, then back to zero. Due to the axes being defined opposite for the Pixhawk and Helmholtz cage, the Pixhawk read the X-axis changing from zero to -250 mG, 250 mG, and back to zero. The left plot shows the cross axis relative to the changing X-axis magnetic field for the Pixhawk Y-axis and Z-axis. The right plot gives a closer look at the Y-axis and Z-axis and their trends.

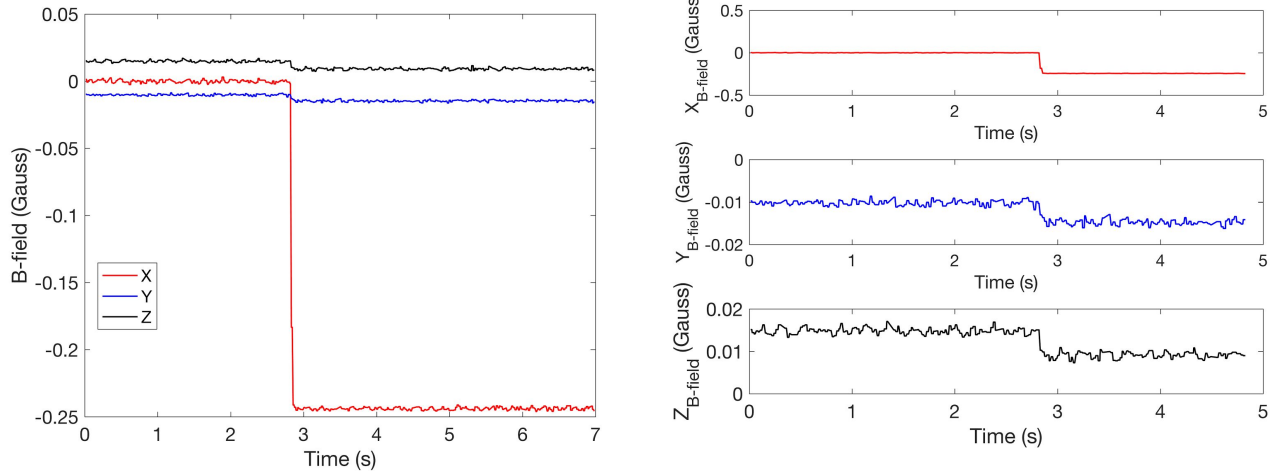


Figure 8: The magnetic field was set at zero, then set at 250 mG in the Helmholtz cage X-axis. Due to the axes being defined opposite for the Pixhawk and Helmholtz cage, the Pixhawk read the X-axis changing from zero to -250 mG. The left plot shows the cross axis relative to the changing X-axis magnetic field for the Pixhawk Y-axis and Z-axis. The right plot gives a closer look at the Y-axis and Z-axis and their trends. One can note a slight shift in time when the magnetometer magnetic field read around -0.18 Gauss in the X-axis.

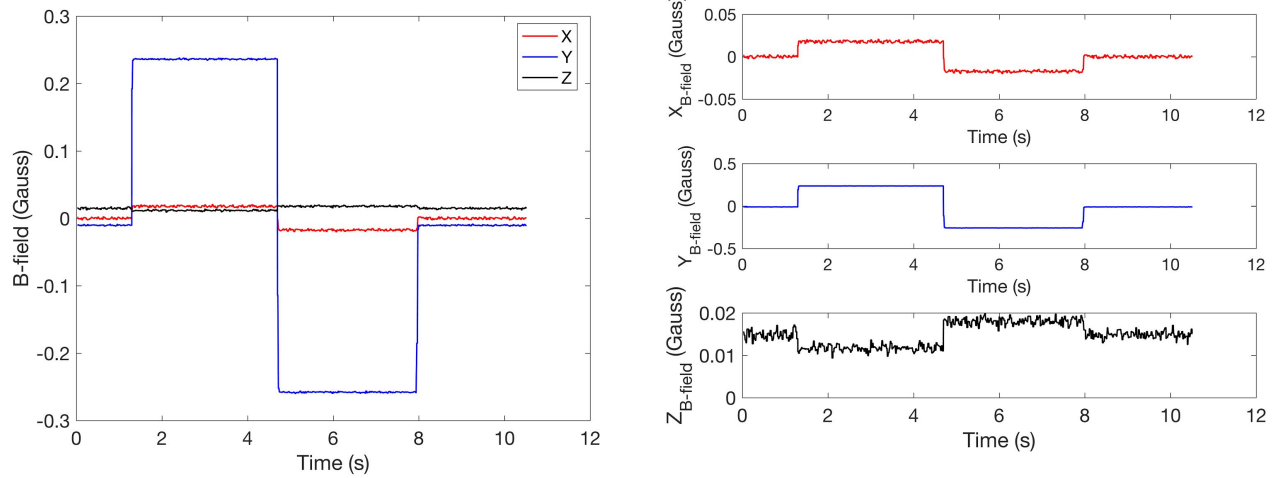


Figure 9: The magnetic field was set at zero, then set at 250 mG in the Helmholtz cage Y-axis, down to -250 mG, then back to zero. The Y-axis was defined the same for the Pixhawk and Helmholtz cage, so the Pixhawk read the Y-axis changing the same way. The left plot shows the cross axis relative to the changing Y-axis magnetic field for the Pixhawk X-axis and Z-axis. The right plot gives a closer look at the X-axis and Z-axis and their trends. Note that the Z-axis changes inversely relative to the Y-axis, causing the cross axis sensitivity, dZ/dY , to be negative. Further analysis is described in Section 5.4.

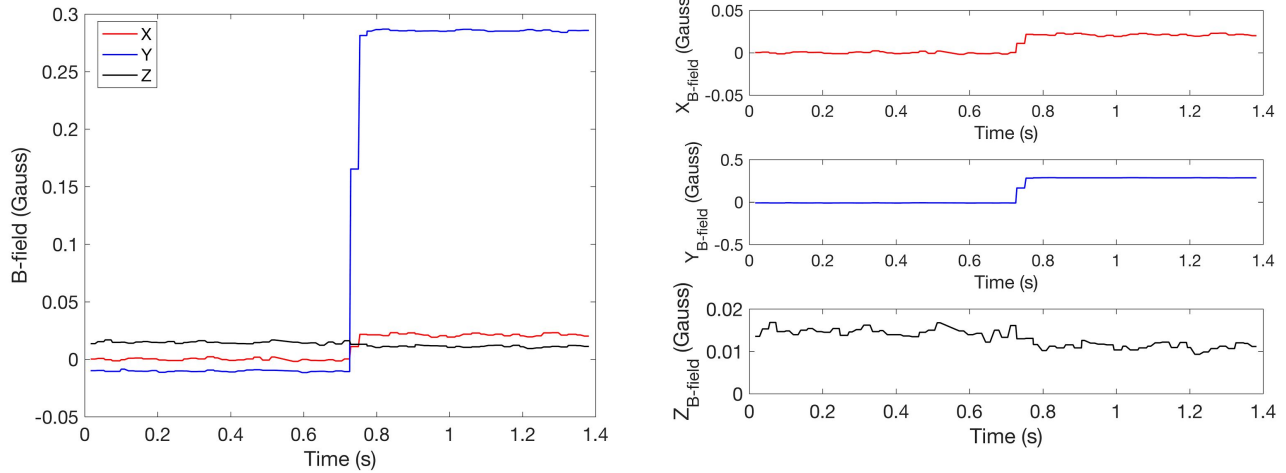


Figure 10: The magnetic field was set at zero, then set at 300 mG in the Helmholtz cage Y-axis. The Y-axis was defined the same for the Pixhawk and Helmholtz cage, so the Pixhawk read the Y-axis changing the same way. The left plot shows the cross axis relative to the changing Y-axis magnetic field for the Pixhawk X-axis and Z-axis. The right plot gives a closer look at the X-axis and Z-axis and their trends. Note the Z-axis shifts down slightly, but is not nearly as noticeably affected as the X-axis. One can note a few shifts in time when the magnetometer magnetic field read around 0.17 Gauss and 0.28 Gauss in the Y-axis.

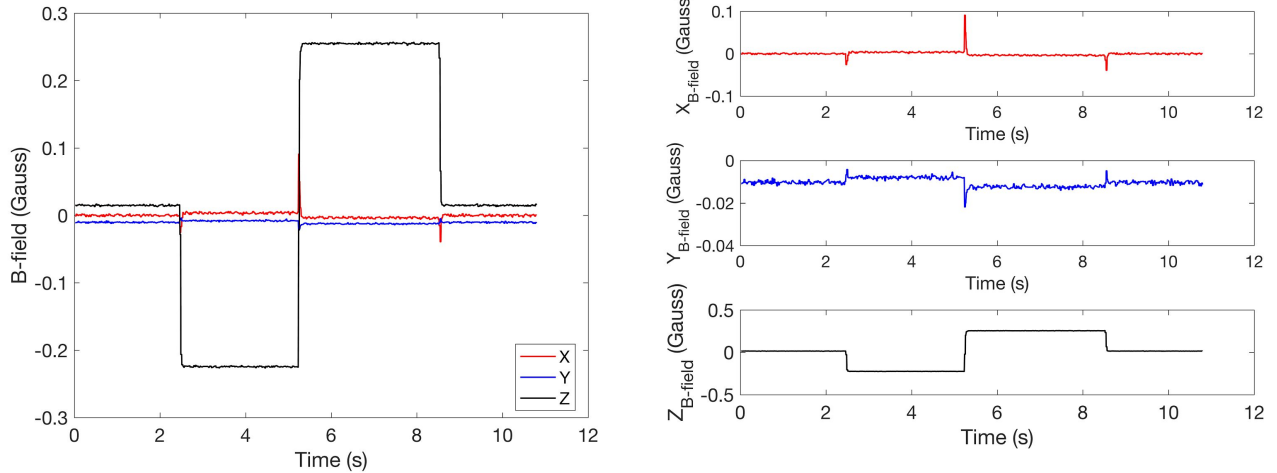


Figure 11: The magnetic field was set at zero, then set at 250 mG in the Helmholtz cage Z-axis, down to -250 mG, then back to zero. Due to the axes being defined opposite for the Pixhawk and Helmholtz cage, the Pixhawk read the Z-axis changing from zero to -250 mG, 250 mG, and back to zero. The left plot shows the cross axis relative to the changing Z-axis magnetic field for the Pixhawk X-axis and Y-axis. The right plot gives a closer look at the X-axis and Z-axis and their trends. This plot looks significantly different than Figures 7 and 9, as the X and Y magnetometer readings don't shift in steps similarly to the Z-axis. Rather, it looks like it shoots and settles at a slightly different value. There is not necessarily an explicable trend for where they settle. Further analysis is described in Section 5.4.

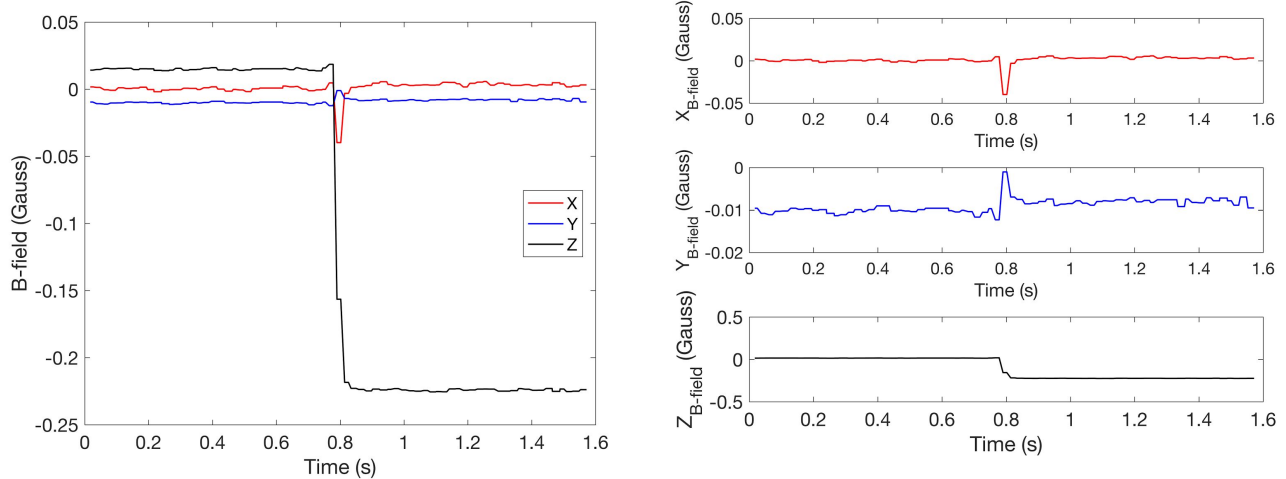


Figure 12: The magnetic field was set at zero, then set at 250 mG in the Helmholtz cage Z-axis. Due to the axes being defined opposite for the Pixhawk and Helmholtz cage, the Pixhawk read the Z-axis changing from zero to -250 mG. The left plot shows the cross axis relative to the changing Z-axis magnetic field for the Pixhawk X-axis and Y-axis. The right plot gives a closer look at the X-axis and Y-axis and their trends. Note the Z-axis shifts down slightly, but is not nearly as noticeably affected as the X-axis. This plot looks significantly different than Figures 8 and 10, as the X and Y magnetometer readings don't shift in steps similarly to the Z-axis. Rather, it looks like it shoots and settles at a slightly different value. There is not necessarily an explicable trend for where they settle. The Z-axis readings also shift in time slightly around -0.17 Gauss and -0.22 Gauss.

Single Axis Changing Magnetic Field Test

Primary writer: Evan Majd

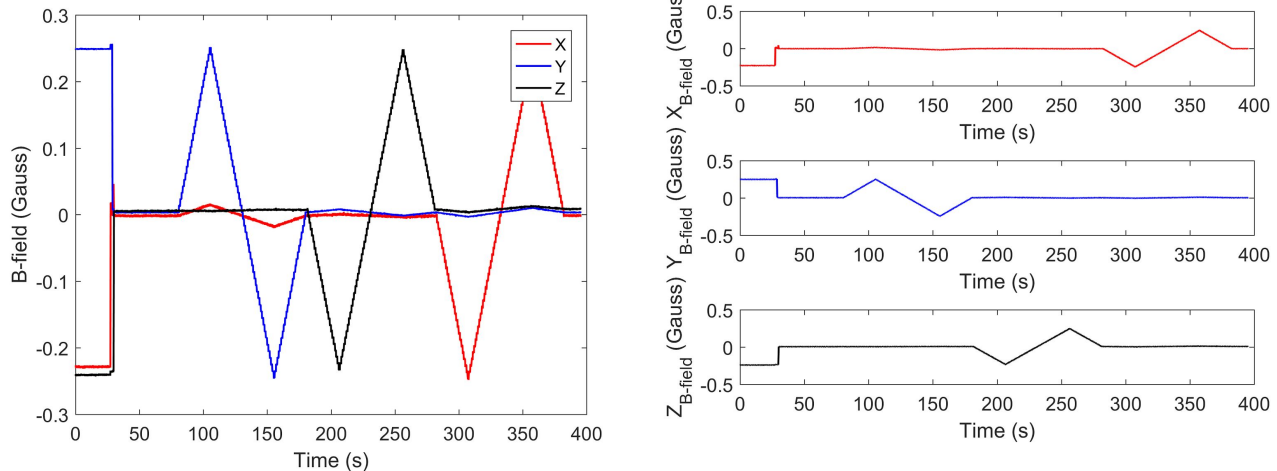


Figure 13: The magnetic field was set to 0 mG, raised up to 250 mG, decreased down to -250 mG, and then brought back to 0 mG. The rate was approximately 10 mG/s. This was run on each axis. The test starts at approximately 30 seconds where the magnetic field on all axis is set to 0 mG. Due to the axes being defined opposite for the Pixhawk and Helmholtz

cage, the Pixhawk reads the X-axis and Z-axis as negative. The left plot shows the cross axis relative to the changing magnetic field. The peaks of the X-axis cross axis have the maximum magnitude of 20.12 mG. The right plot gives a closer look of the separate axis measurements.

Single Axis Rotating Magnetic Field Test

Primary writer: Evan Majd

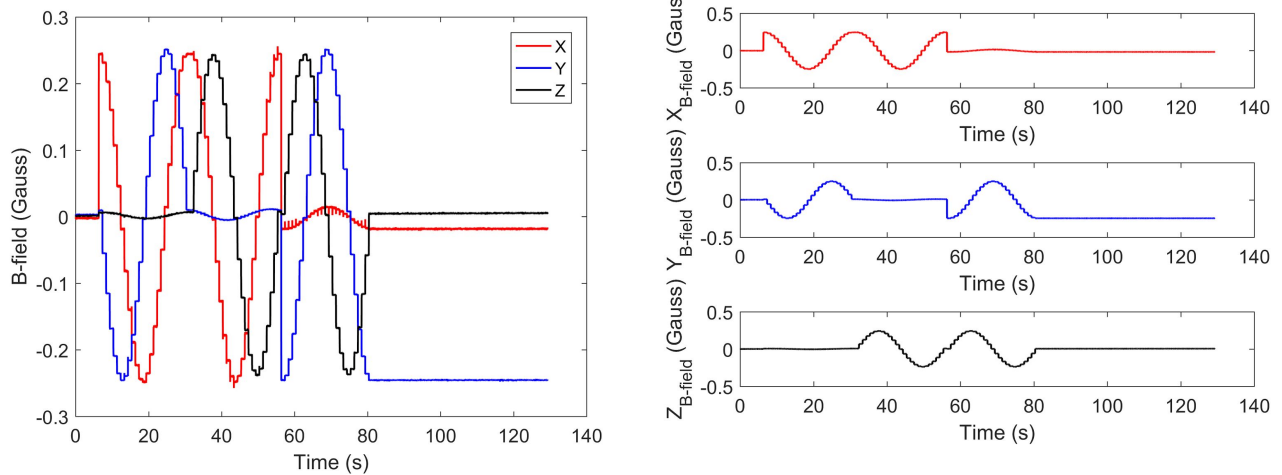


Figure 14: The magnetic field was set to 250 mG and was rotated about each axis in steps of approximately 15 °/s. The axis of rotation was at 0 mG. The test starts at approximately 7 seconds where the magnetic field on all axis all start at zero. Due to the axes being defined opposite for the Pixhawk and Helmholtz cage, the Pixhawk reads the X-axis and Z-axis as negative. The left plot shows the cross axis relative to the changing magnetic field. The peaks of the X-axis cross axis have the maximum magnitude of 20.52 mG. The right plot gives a closer look of the separate axis measurements.

A2. Plate Rotation in a Constant Magnetic Field

X-Axis 0 mG Magnetic Field with Rotating Plate Test

Primary writer: Evan Majd

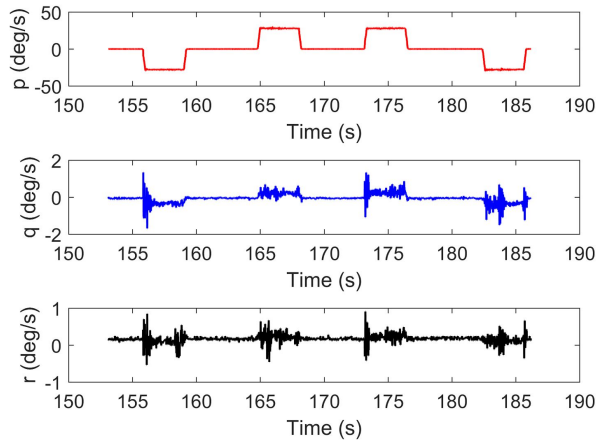


Figure 15: The magnetic field was set to 0 mG, and was rotated about the X-axis from 0 deg to 90 deg, back to 0 deg, down to -90 deg and back to 0 deg. The rate of rotation was approximately 28 °/sec. Due to the axes being defined opposite for the Pixhawk and Helmholtz cage, the Pixhawk reads the X-axis as negative. The plot also shows spikes in the q and r gyroscope measurement when rotations were occurring.

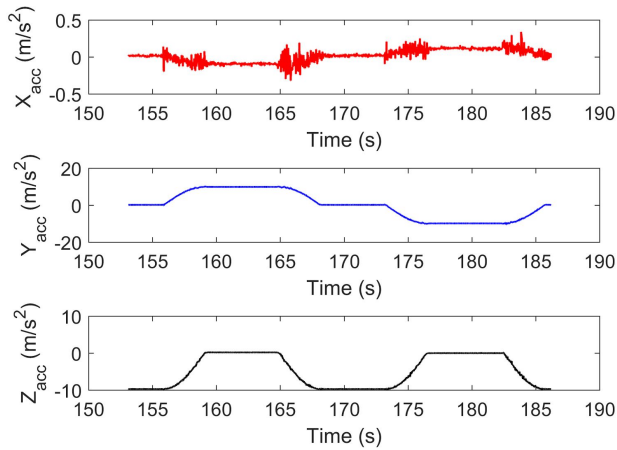


Figure 16: The magnetic field was set to 0 mG, and was rotated about the X-axis from 0 deg to 90 deg, back to 0 deg, down to -90 deg and back to 0 deg. The rate of rotation was approximately 28 °/sec. Due to the axes being defined opposite for the Pixhawk and Helmholtz cage, the Pixhawk reads the X-axis as negative. The acceleration of gravity is measured between the Y-axis and X-axis for this rotation.

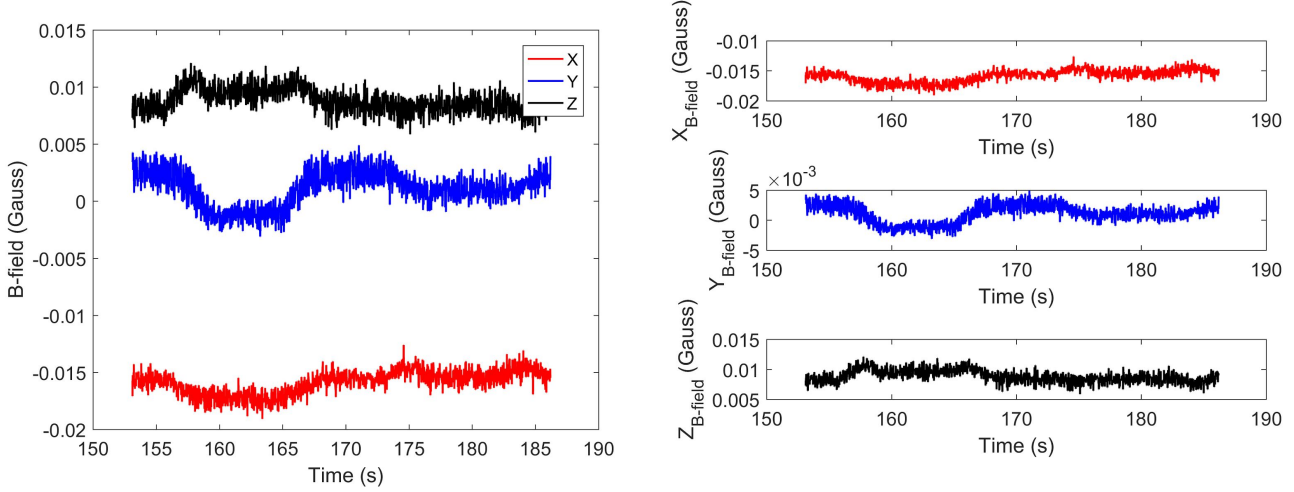


Figure 17: The magnetic field was set to 0 mG and was rotated about the X-axis in steps of approximately $15^{\circ}/\text{s}$. The axis of rotation was at 0 mG. Due to the axes being defined opposite for the Pixhawk and Helmholtz cage, the Pixhawk reads the X-axis as negative. The left plot shows the cross axis relative to the changing magnetic field. The right plot gives a closer look of the separate axis measurements.

Y-Axis 0 mG Magnetic Field with Rotating Plate Test

Primary writer: Evan Majd

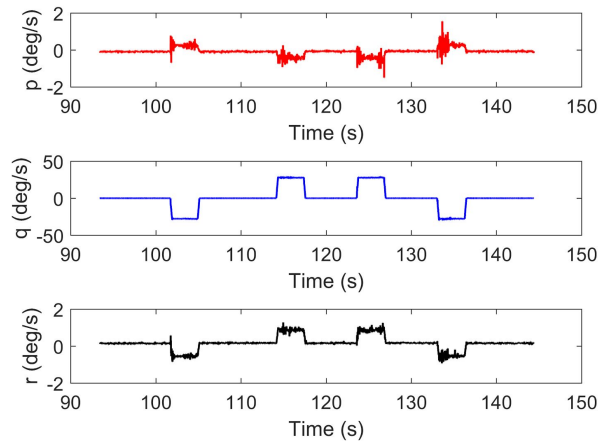


Figure 18: The magnetic field was set to 0 mG, and was rotated about the Y-axis from 0 deg to 90 deg, back to 0 deg, down to -90 deg and back to 0 deg. The rate of rotation was approximately $28^{\circ}/\text{sec}$. The plot shows spikes in the p and r gyroscope measurement when rotations were occurring.

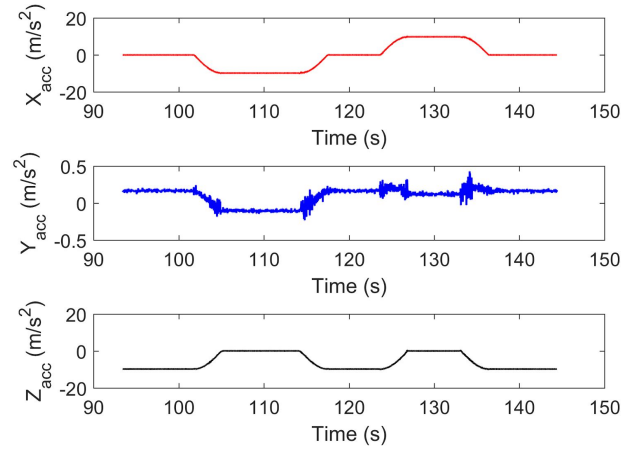


Figure 19: The magnetic field was set to 0 mG, and was rotated about the Y-axis from 0 deg to 90 deg, back to 0 deg, down to -90 deg and back to 0 deg. The rate of rotation was approximately $28^{\circ}/\text{sec}$. The acceleration of gravity is measured between the X-axis and Z-axis for this rotation.

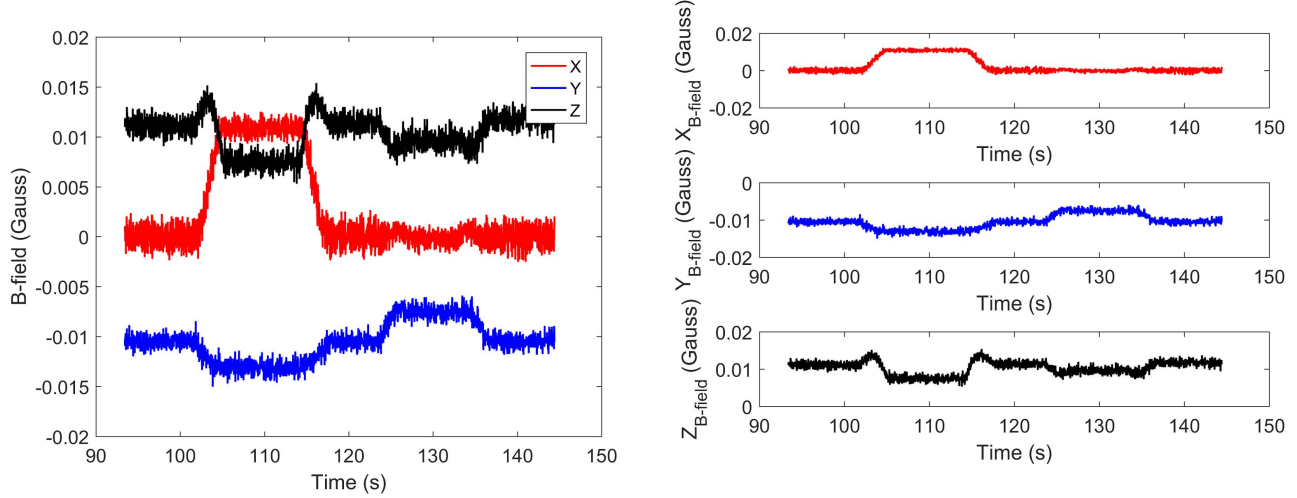


Figure 20: The magnetic field was set to 0 mG and was rotated about the Y-axis in steps of approximately $15^{\circ}/\text{s}$. The axis of rotation was at 0 mG. The left plot shows the cross axis relative to the changing magnetic field. The right plot gives a closer look of the separate axis measurements.

Z-Axis 0 mG Magnetic Field with Rotating Plate Test

Primary writer: Evan Majd

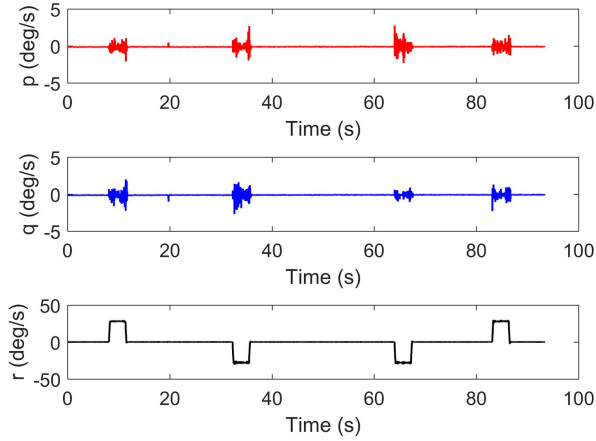


Figure 21: The magnetic field was set to 0 mG, and was rotated about the Z-axis from 0 deg to 90 deg, back to 0 deg, down to -90 deg and back to 0 deg. The rate of rotation was approximately 28 °/sec. Due to the axes being defined opposite for the Pixhawk and Helmholtz cage, the Pixhawk reads the Z-axis as negative. The plot also shows spikes in the p and q gyroscope measurement when rotations were occurring.

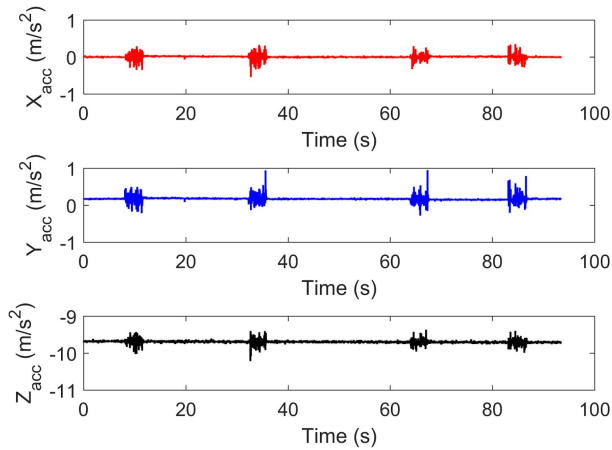


Figure 22: The magnetic field was set to 0 mG, and was rotated about the Z-axis from 0 deg to 90 deg, back to 0 deg, down to -90 deg and back to 0 deg. The rate of rotation was approximately 28 °/sec. Due to the axes being defined opposite for the Pixhawk and Helmholtz cage, the Pixhawk reads the Z-axis as negative. The acceleration of gravity is measured in the Z-axis for this rotation.

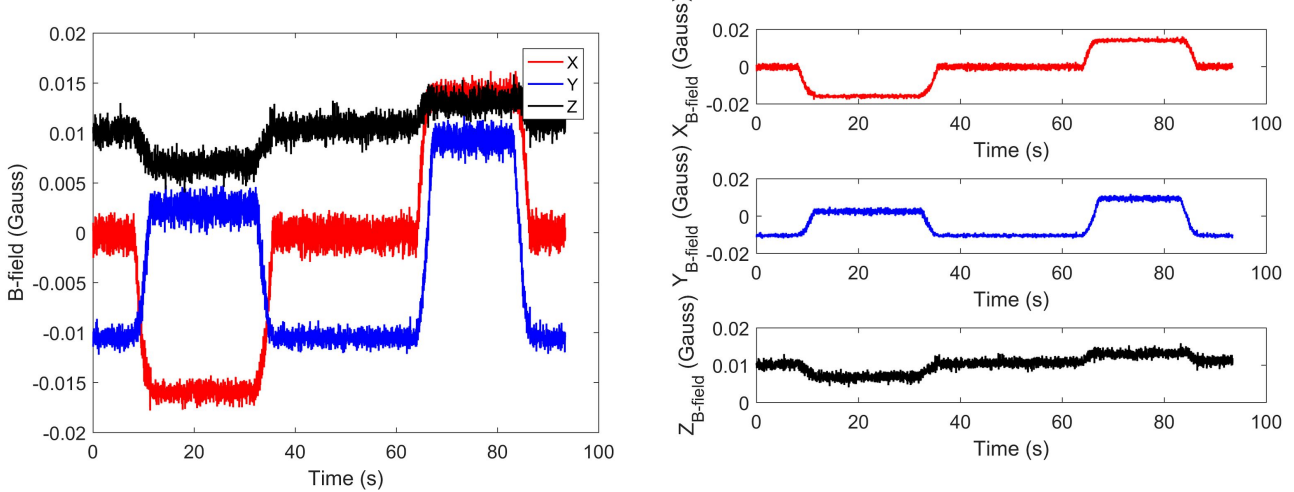


Figure 23: The magnetic field was set to 0 mG and was rotated about the Z-axis in steps of approximately $15^{\circ}/s$. The axis of rotation was at 0 mG. Due to the axes being defined opposite for the Pixhawk and Helmholtz cage, the Pixhawk reads the Z-axis as negative. The left plot shows the cross axis relative to the changing magnetic field. The right plot gives a closer look of the separate axis measurements.

X-Axis 250 mG Magnetic Field with Rotating Plate Test

Primary writer: Evan Majd

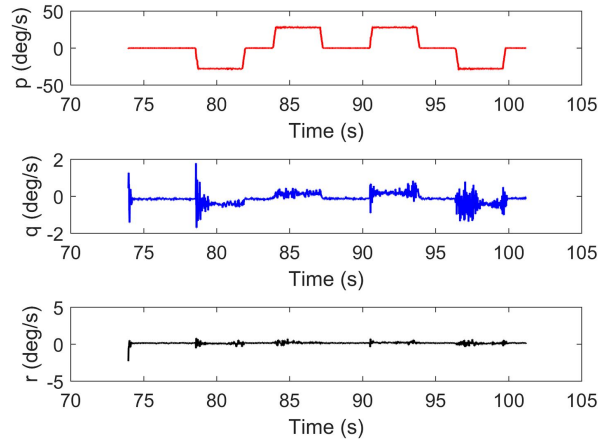


Figure 24: The magnetic field was set to 250 mG, and was rotated about the X-axis from 0 deg to 90 deg, back to 0 deg, down to -90 deg and back to 0 deg. The rate of rotation was approximately $28^{\circ}/\text{sec}$. Due to the axes being defined opposite for the Pixhawk and Helmholtz cage, the Pixhawk reads the X-axis as negative. The plot also shows spikes in the q and r gyroscope measurement when rotations were occurring.

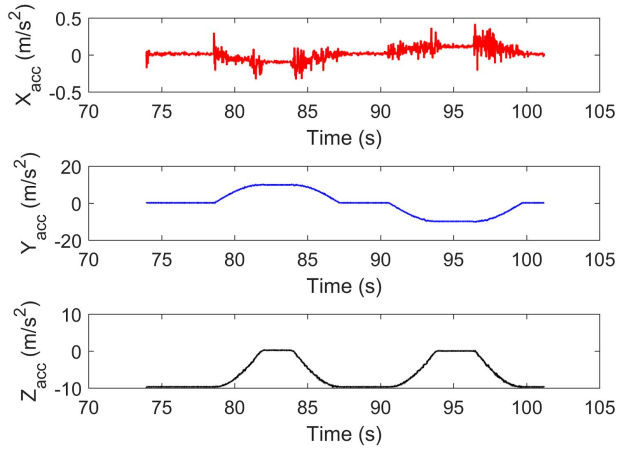


Figure 25: The magnetic field was set to 250 mG, and was rotated about the X-axis from 0 deg to 90 deg, back to 0 deg, down to -90 deg and back to 0 deg. The rate of rotation was approximately $28^\circ/\text{sec}$. Due to the axes being defined opposite for the Pixhawk and Helmholtz cage, the Pixhawk reads the X-axis as negative. The acceleration of gravity is measured between the Y-axis and Z-axis for this rotation.

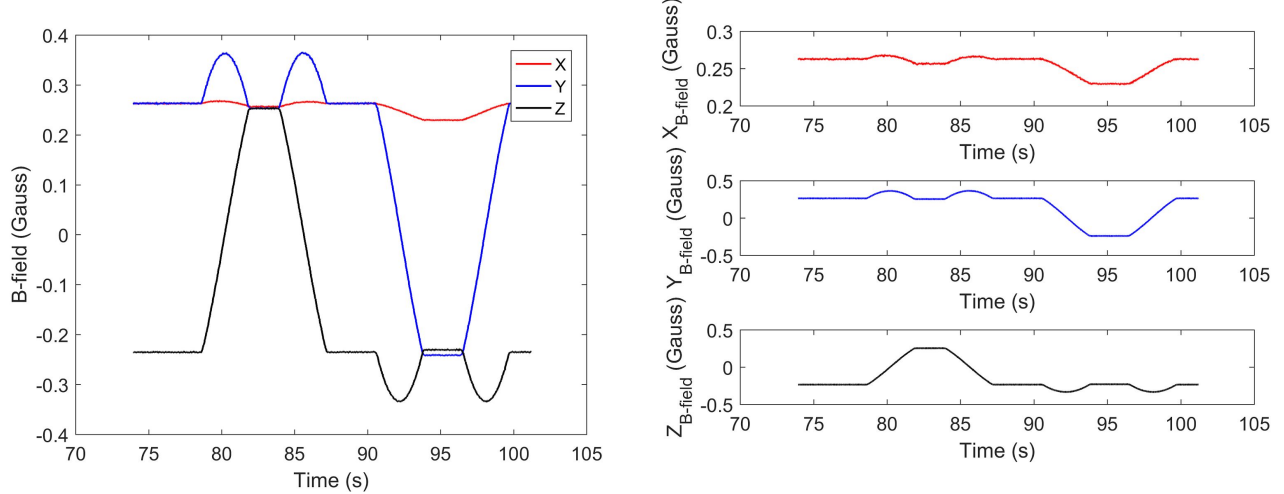


Figure 26: The magnetic field was set to 250 mG and was rotated about the X-axis in steps of approximately $15^\circ/\text{s}$. Due to the axes being defined opposite for the Pixhawk and Helmholtz cage, the Pixhawk reads the X-axis as negative. The left plot shows the cross axis relative to the changing magnetic field. The right plot gives a closer look of the separate axis measurements.

Y-Axis 250 mG Magnetic Field with Rotating Plate Test

Primary writer: Evan Majd

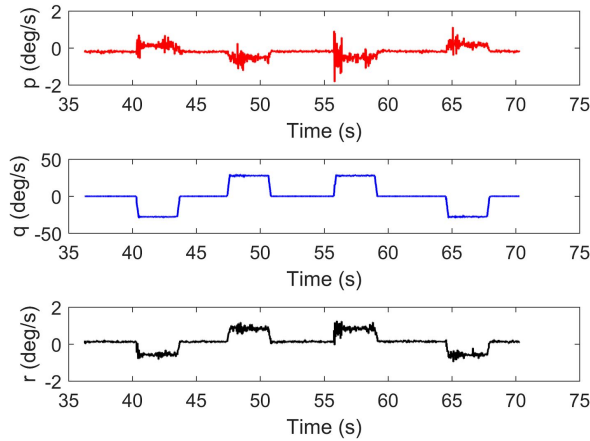


Figure 27: The magnetic field was set to 250 mG, and was rotated about the Y-axis from 0 deg to 90 deg, back to 0 deg, down to -90 deg and back to 0 deg. The rate of rotation was approximately 28 °/sec. The plot shows spikes in the p and r gyroscope measurement when rotations were occurring.

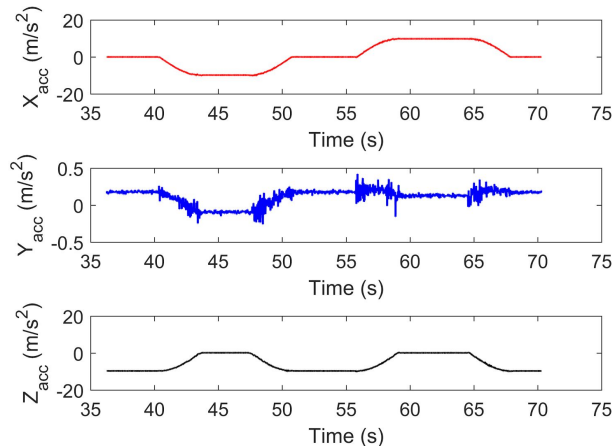


Figure 28: The magnetic field was set to 250 mG, and was rotated about the Y-axis from 0 deg to 90 deg, back to 0 deg, down to -90 deg and back to 0 deg. The rate of rotation was approximately 28 °/sec. The acceleration of gravity is measured between the X-axis and Z-axis for this rotation.

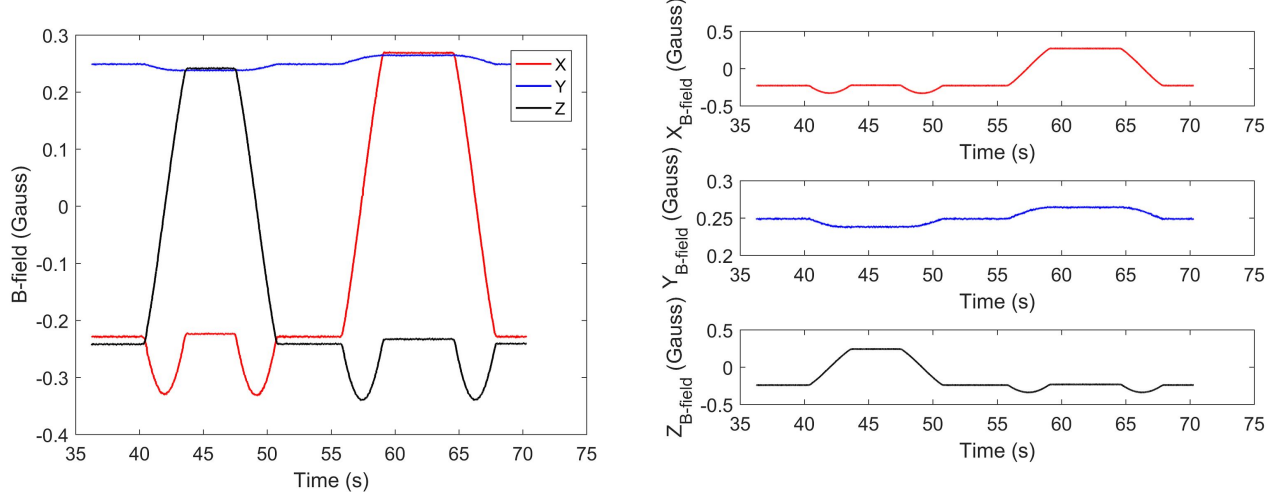


Figure 29: The magnetic field was set to 250 mG and was rotated about the Y-axis in steps of approximately $15^{\circ}/s$. The left plot shows the cross axis relative to the changing magnetic field. The right plot gives a closer look of the separate axis measurements.

Z-Axis 250 mG Magnetic Field with Rotating Plate Test

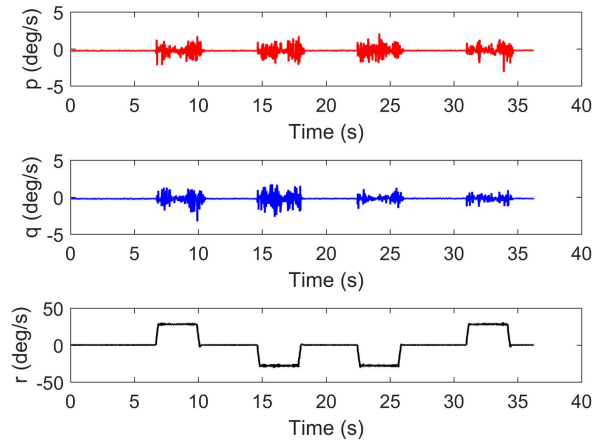


Figure 30: The magnetic field was set to 250 mG, and was rotated about the Z-axis from 0 deg to 90 deg, back to 0 deg, down to -90 deg and back to 0 deg. The rate of rotation was approximately $28^{\circ}/sec$. Due to the axes being defined opposite for the Pixhawk and Helmholtz cage, the Pixhawk reads the Z-axis as negative. The plot also shows spikes in the p and q gyroscope measurement when rotations were occurring.

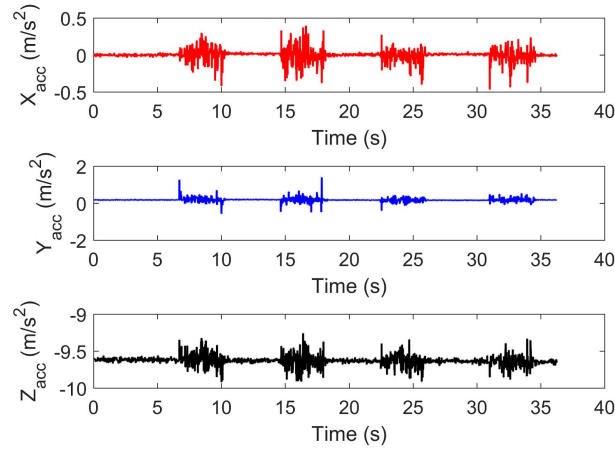


Figure 31: The magnetic field was set to 250 mG, and was rotated about the Z-axis from 0 deg to 90 deg, back to 0 deg, down to -90 deg and back to 0 deg. The rate of rotation was approximately $28^{\circ}/\text{sec}$. Due to the axes being defined opposite for the Pixhawk and Helmholtz cage, the Pixhawk reads the Z-axis as negative. The acceleration of gravity is measured in the Z-axis for this rotation.

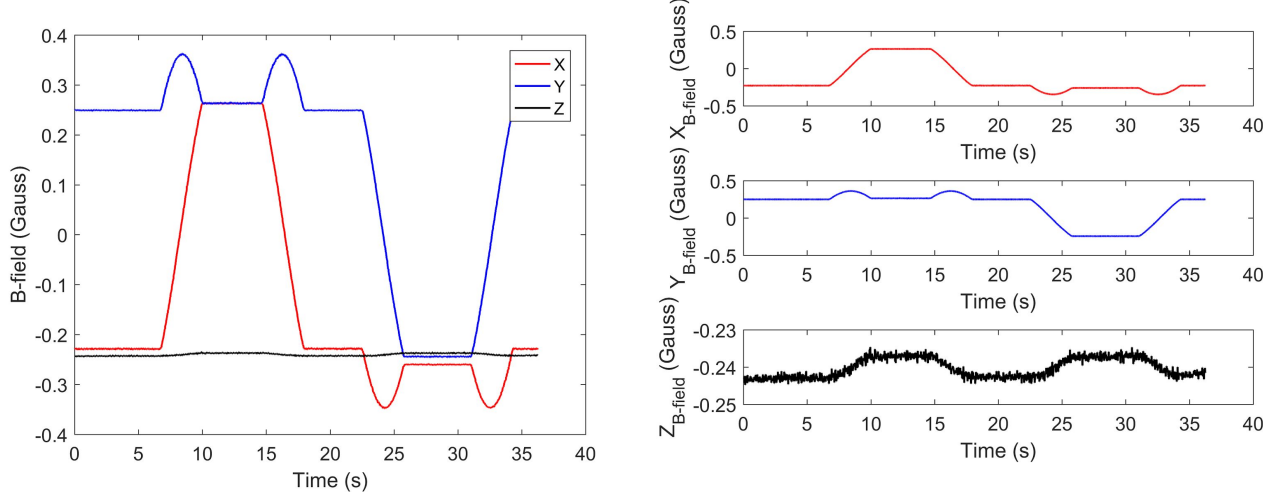


Figure 32: The magnetic field was set to 250 mG and was rotated about the Z-axis in steps of approximately $15^{\circ}/\text{s}$. Due to the axes being defined opposite for the Pixhawk and Helmholtz cage, the Pixhawk reads the Z-axis as negative. The left plot shows the cross axis relative to the changing magnetic field. The right plot gives a closer look of the separate axis measurements.

X-axis Constant “On-Orbit” Magnetic Field with Rotating Plate Test

Primary writer: Lindsay Taylor

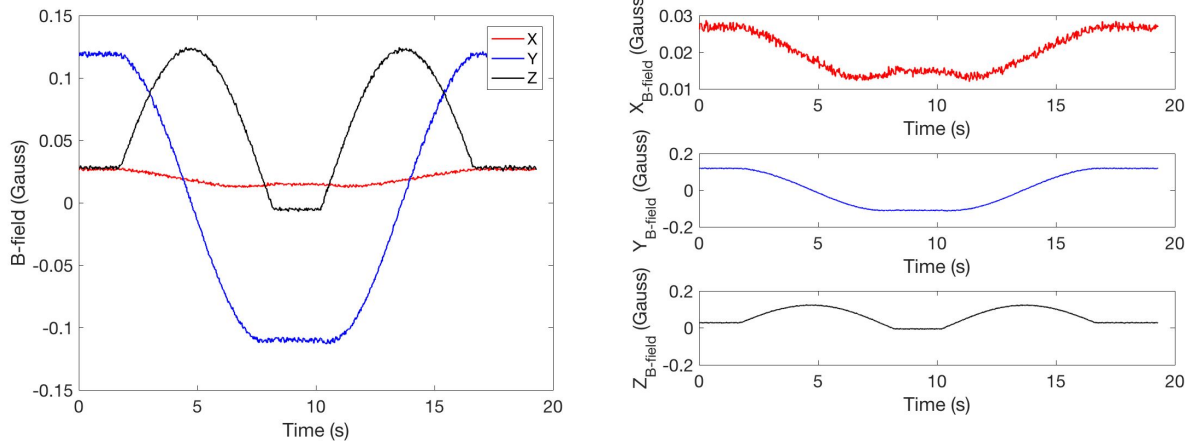


Figure 33: The magnetic field was set to an on-orbit coordinate at a magnitude of 255.93 mG and was rotated about the X-axis at approximately $28^{\circ}/\text{sec}$. The plate was rotated from -90° to $+90^{\circ}$ and then brought back to its initial location. The axis of rotation was at 226.44 mG. The left plot demonstrates the interactions between each axis, while the right plot gives a closer look at each individual axis.

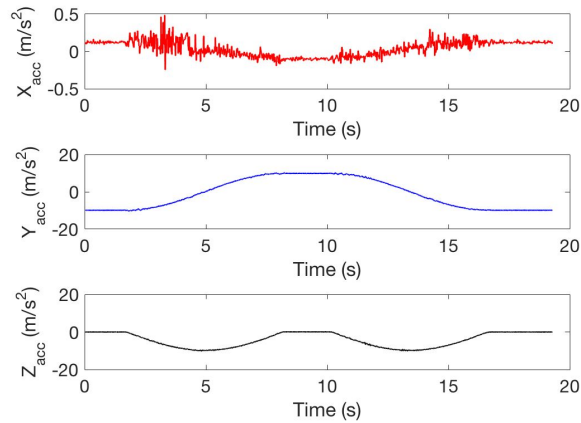


Figure 34: Accelerometer readings from the Pixhawk that is being rotated about the X-axis in a constant on-orbit magnetic field. The field was set to a specific coordinate at a magnitude of 255.93 mG. The plate was rotated from -90° to $+90^{\circ}$ and then brought back to its initial location. The accelerations are measured between the Y-axis and Z-axis for this rotation.

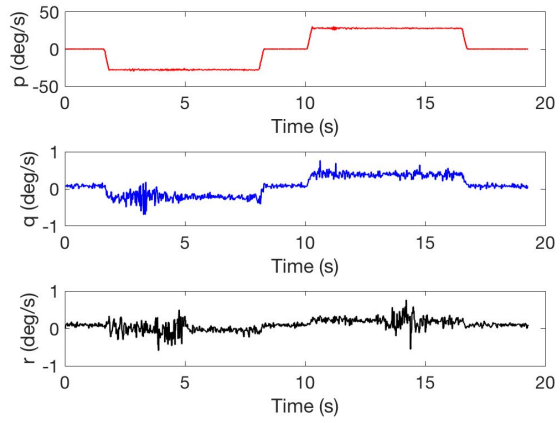


Figure 35: Gyroscope readings from the Pixhawk that is being rotated about the X-axis in a constant on-orbit magnetic field. The field was set to a specific coordinate at a magnitude of 255.93 mG. The plate was rotated from -90° to $+90^\circ$ and then brought back to its initial location.

Y-axis Constant On-orbit Magnetic Field with Rotating Plate Test

Primary writer: Lindsay Taylor

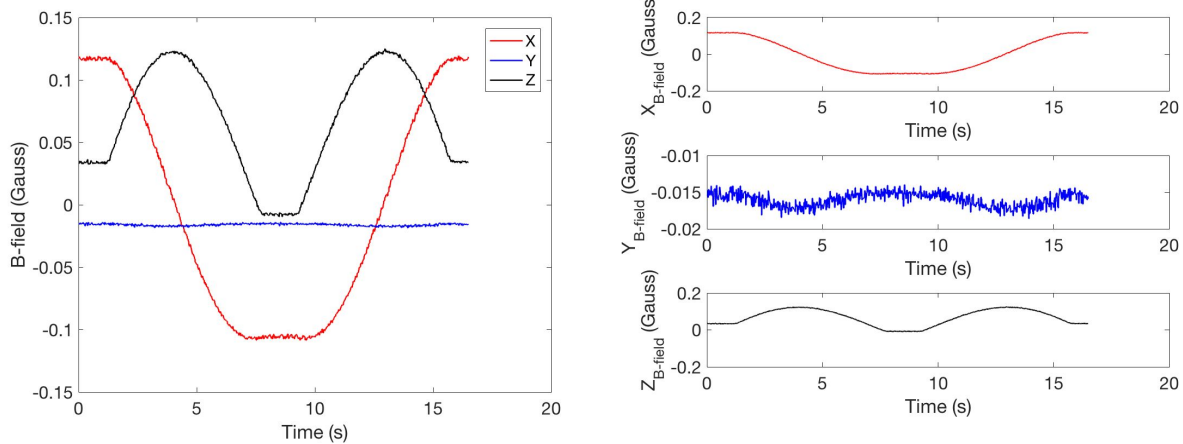


Figure 36: The magnetic field was set to an on-orbit coordinate at a magnitude of 255.93 mG and was rotated about the Y-axis at approximately $28^\circ/\text{sec}$. The plate was rotated from -90° to $+90^\circ$ and then brought back to its initial location. The axis of rotation was at -21.06 mG. The left plot demonstrates the interactions between each axis, while the right plot gives a closer look at each individual axis.

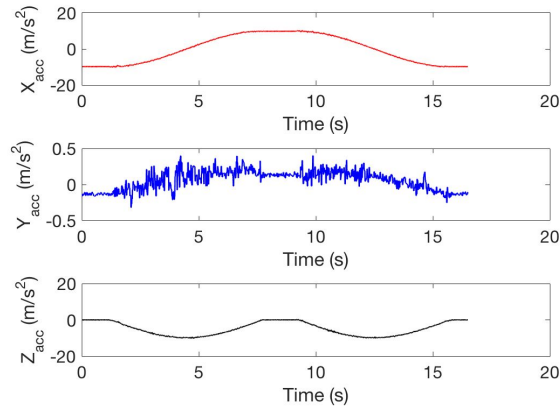


Figure 37: Accelerometer readings from the Pixhawk that is being rotated about the Y-axis in a constant on-orbit magnetic field. The field was set to a specific coordinate at a magnitude of 255.93 mG. The plate was rotated from -90° to $+90^\circ$ and then brought back to its initial location. The accelerations are measured between the X-axis and Z-axis for this rotation.

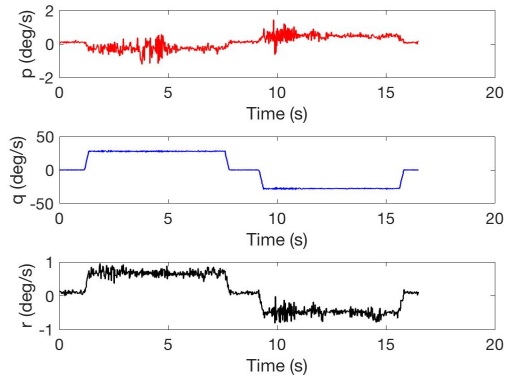


Figure 38: Gyroscope readings from the Pixhawk that is being rotated about the Y-axis in a constant on-orbit magnetic field. The field was set to a specific coordinate at a magnitude of 255.93 mG. The plate was rotated from -90° to $+90^\circ$ and then brought back to its initial location.

Z-axis Constant On-orbit Magnetic Field with Rotating Plate Test

Primary writer: Lindsay Taylor

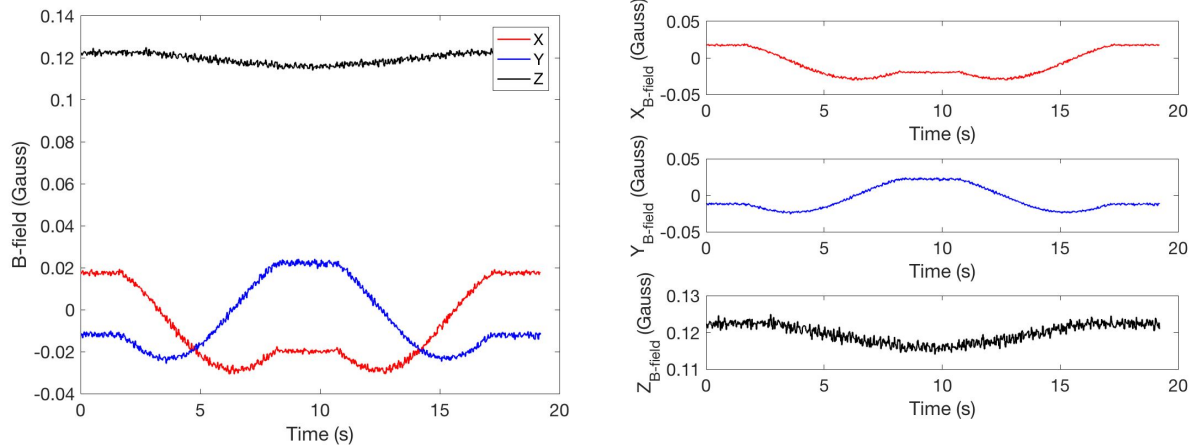


Figure 39: The magnetic field was set to an on-orbit coordinate at a magnitude of 255.93 mG and was rotated about the Z-axis at approximately $28^{\circ}/\text{sec}$. The plate was rotated from -90° to $+90^{\circ}$ and then brought back to its initial location. The axis of rotation was at -117.39 mG. The left plot demonstrates the interactions between each axis, while the right plot gives a closer look at each individual axis.

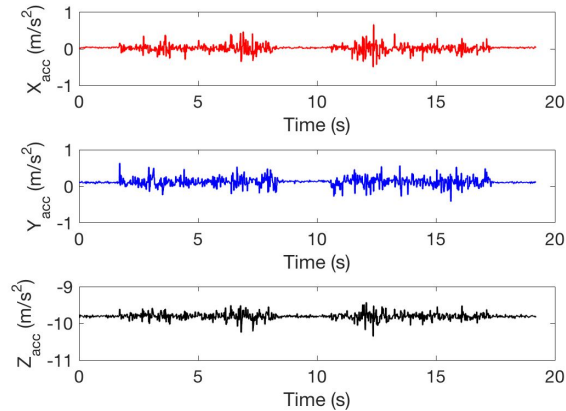


Figure 40: Accelerometer readings from the Pixhawk that is being rotated about the Z-axis in a constant on-orbit magnetic field. The field was set to a specific coordinate at a magnitude of 255.93 mG. The plate was rotated from -90° to $+90^{\circ}$ and then brought back to its initial location. The acceleration is measured solely in the Z-axis for this rotation.

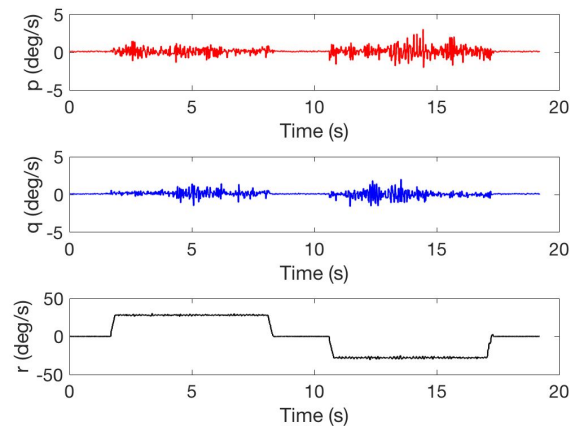


Figure 41: Gyroscope readings from the Pixhawk that is being rotated about the Z-axis in a constant on-orbit magnetic field. The field was set to a specific coordinate at a magnitude of 255.93 mG. The plate was rotated from -90° to $+90^\circ$ and then brought back to its initial location.

A3. Rotating Magnetic Field with Rotating Plate Tests

Primary writer: Stephanie Wegner

X-Axis Rotation

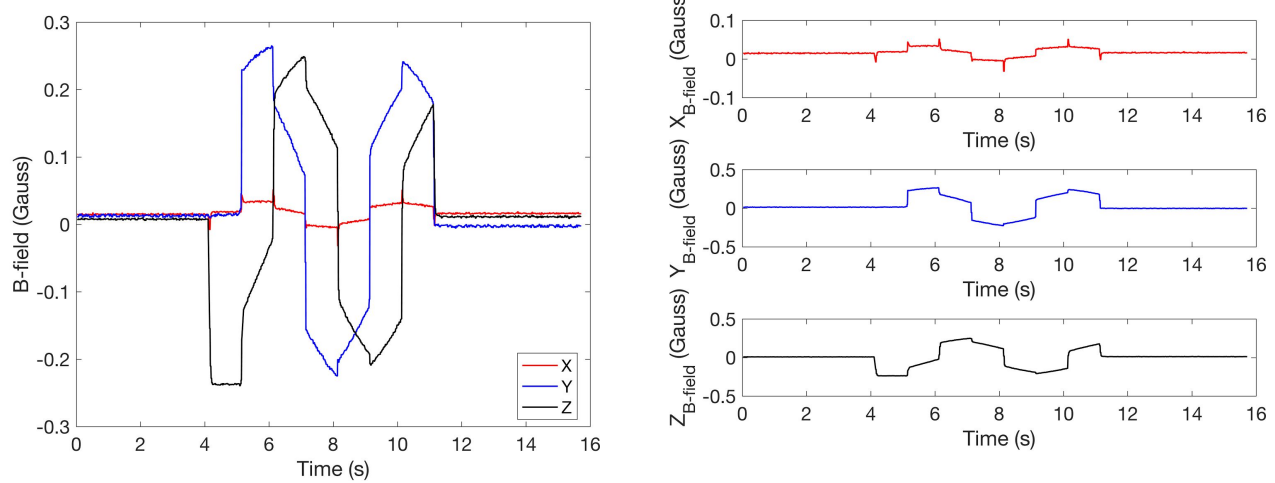


Figure 42: The magnetometer data is shown for when magnetic field was rotated 360 degrees about the Pixhawk X-axis while the plate was also rotated 180 degrees about the same axis. The plot on the right also gives a closer look at interference or cross axis sensitivity displayed in the X-axis.

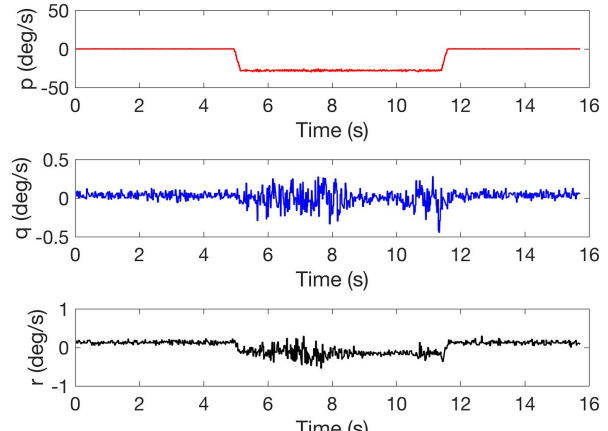
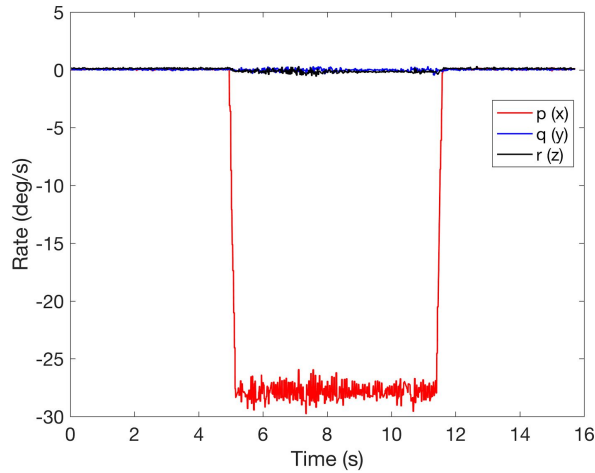


Figure 43: The gyroscope data is shown for when magnetic field was rotated 360 degrees about the Pixhawk X-axis while the plate was also rotated 180 degrees about the same axis. The plot on the right gives a closer look at interference or sensitivity displayed in the Y and Z axes.

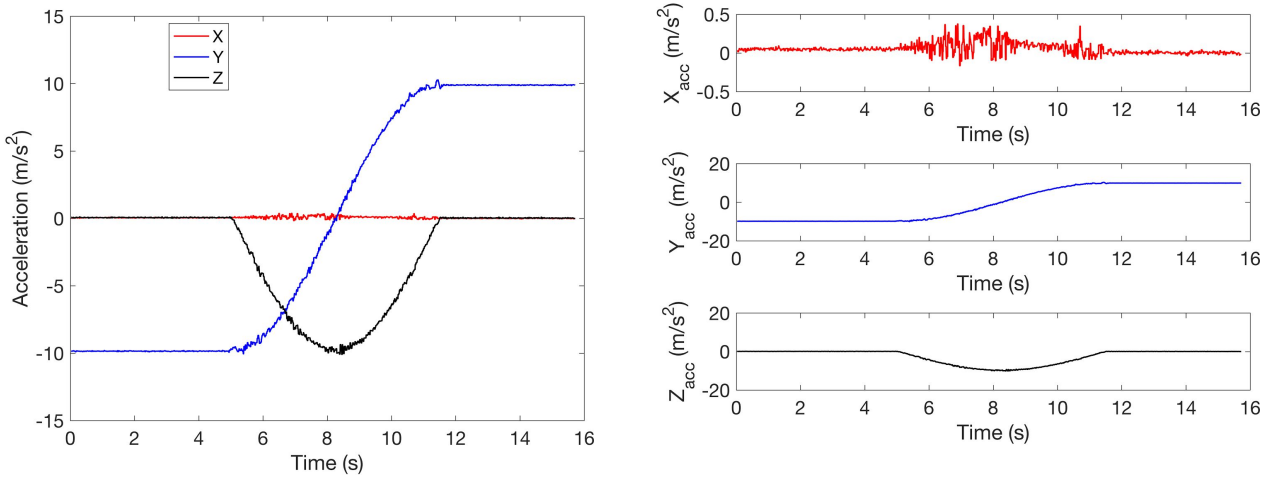


Figure 44: The gyroscope data is shown for when magnetic field was rotated 360 degrees about the Pixhawk X-axis while the plate was also rotated 180 degrees about the same axis. The plot on the right gives a closer look at the sensitivity displayed in the X-axis.

Y-Axis Rotation

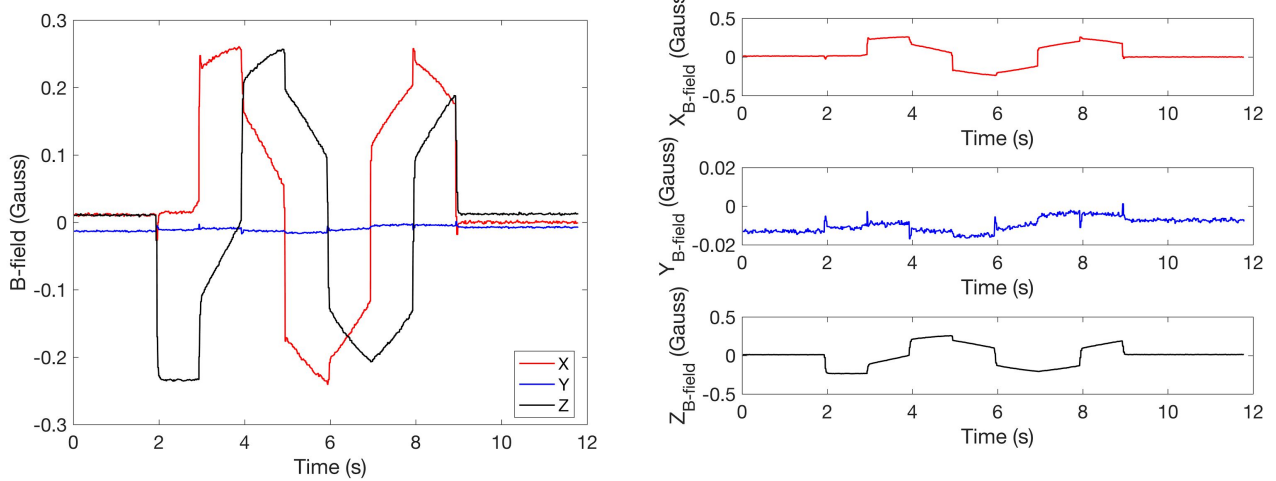


Figure 45: The magnetometer data is shown for when magnetic field was rotated 360 degrees about the Pixhawk Y-axis while the plate was also rotated 180 degrees about the same axis. The plot on the right also gives a closer look at interference or cross axis sensitivity displayed in the Y-axis.

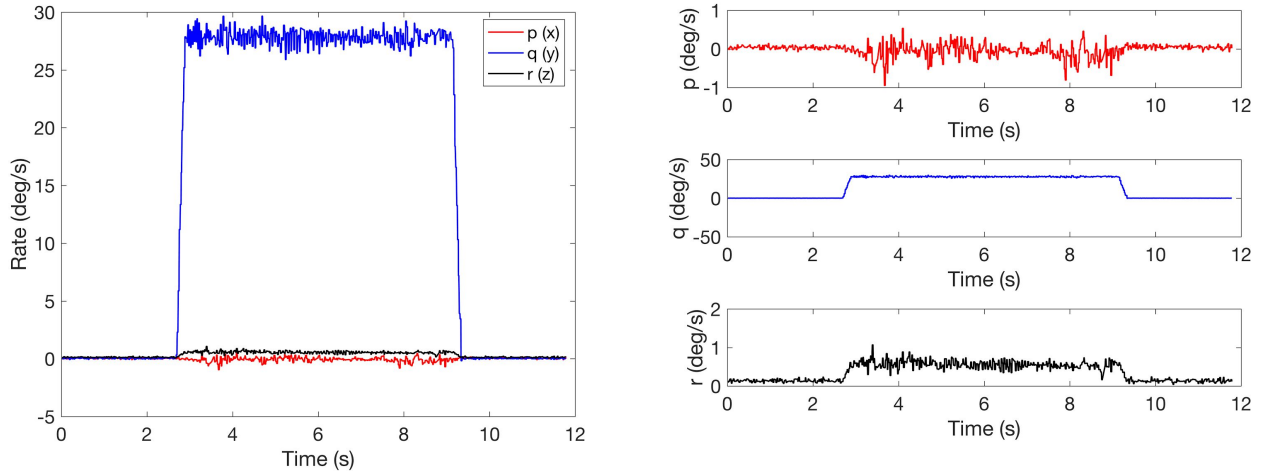


Figure 46: The gyroscope data is shown for when magnetic field was rotated 360 degrees about the Pixhawk Y-axis while the plate was also rotated 180 degrees about the same axis. The plot on the right gives a closer look at interference or sensitivity displayed in the X and Z axes.

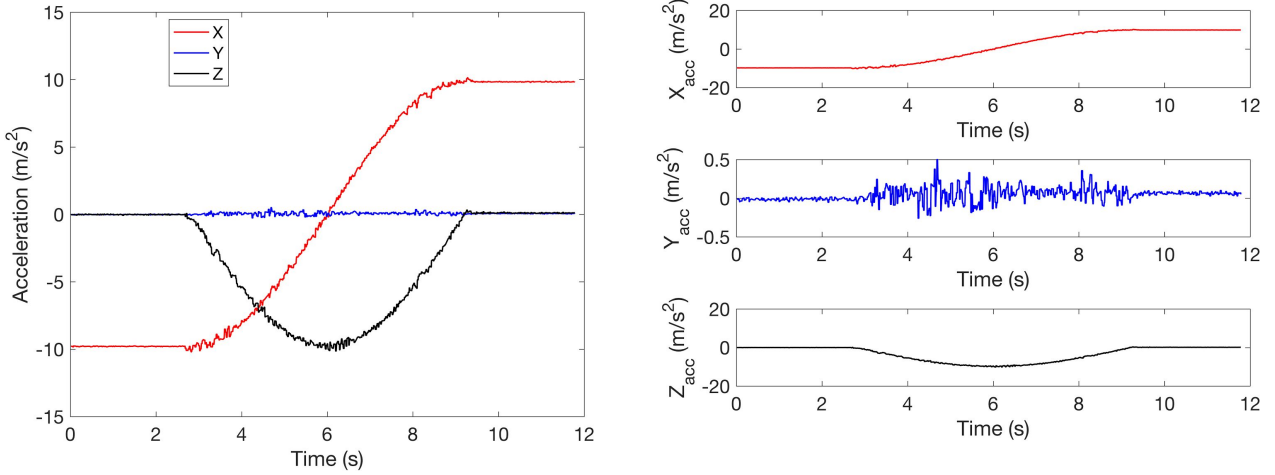


Figure 47: The gyroscope data is shown for when magnetic field was rotated 360 degrees about the Pixhawk Y-axis while the plate was also rotated 180 degrees about the same axis. The plot on the right gives a closer look at the sensitivity displayed in the Y-axis.

Z-Axis Rotation

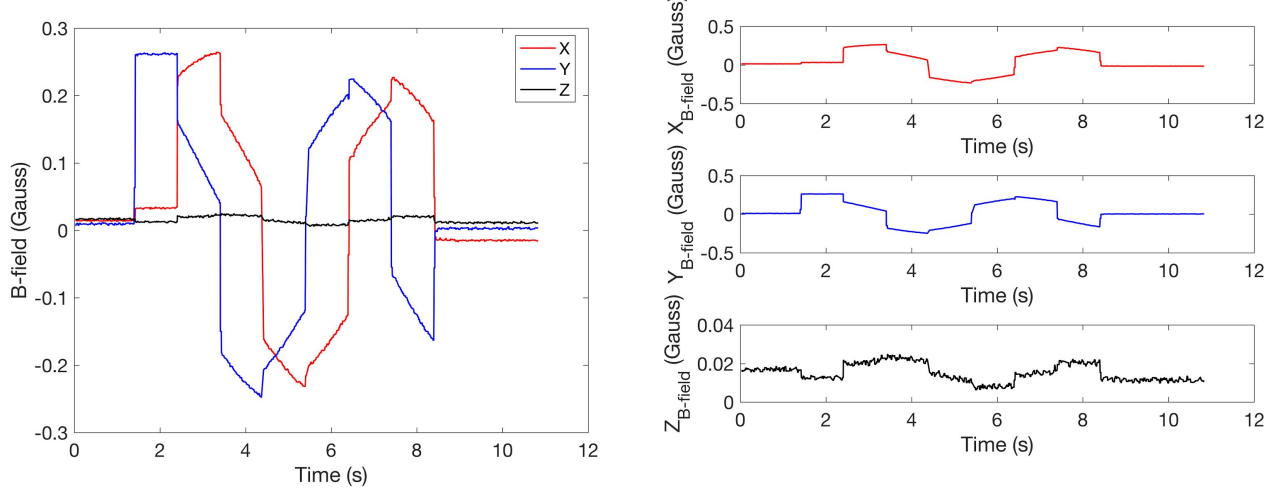


Figure 48: The magnetometer data is shown for when magnetic field was rotated 360 degrees about the Pixhawk Z-axis while the plate was also rotated 180 degrees about the same axis. The plot on the right also gives a closer look at interference or cross axis sensitivity displayed in the Z-axis.

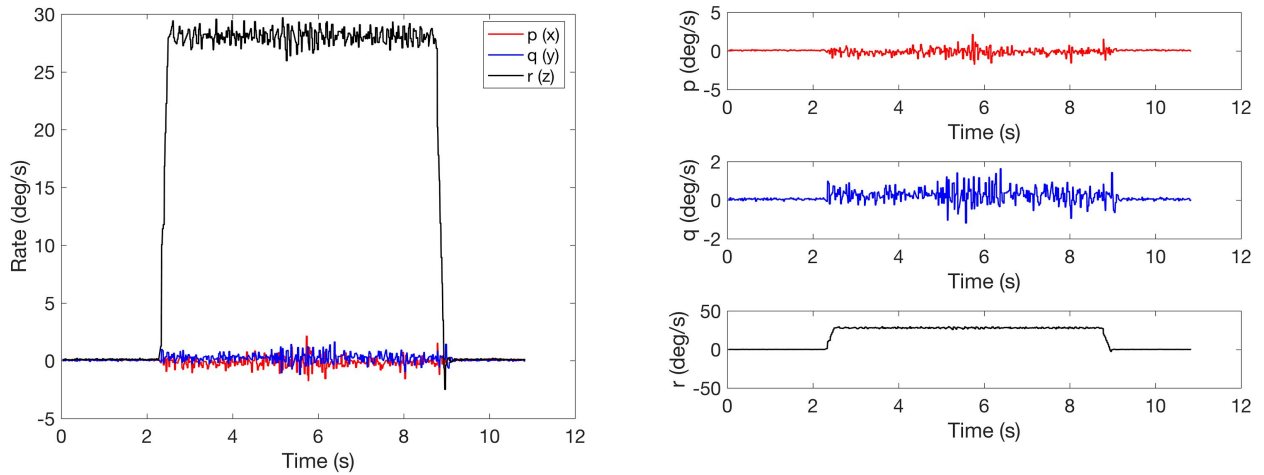


Figure 49: The gyroscope data is shown for when magnetic field was rotated 360 degrees about the Pixhawk Z-axis while the plate was also rotated 180 degrees about the same axis. The plot on the right gives a closer look at interference or sensitivity displayed in the X and Y axes.

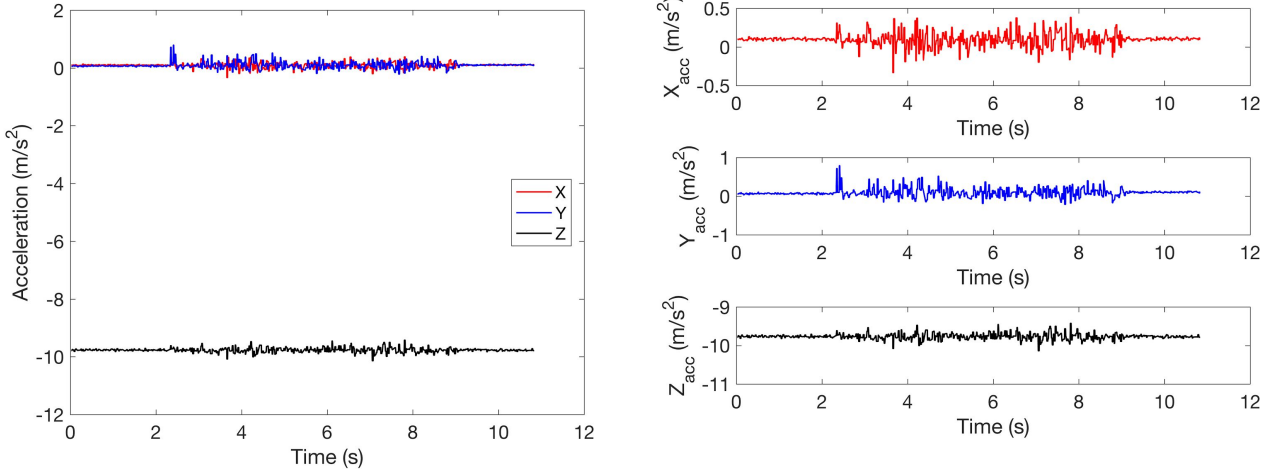


Figure 50: The gyroscope data is shown for when magnetic field was rotated 360 degrees about the Pixhawk Z-axis while the plate was also rotated 180 degrees about the same axis. The plot on the right gives a closer look at the sensitivity displayed in each axis. Note that these figures for acceleration look significantly different than Figures 44 and 47 because the plate was rotated about an axis parallel to the gravity acceleration vector, and the X and Y plate rotations were about an axis perpendicular to the gravity acceleration vector.

A4. Zero-Gauss Chamber Tests

Three Layer Zero Gauss Chamber Tests

Primary writer: Lindsay Taylor

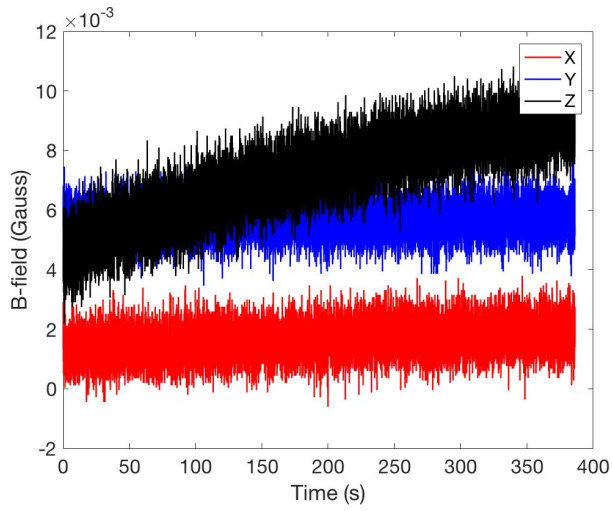


Figure 51: Pixhawk magnetometer readings from the three layer Zero Gauss Chamber lying horizontally without the cap on. The high drift rate from the Z-magnetometer is witnessed in this figure. This data was used in calculating magnetometer drift and bias.

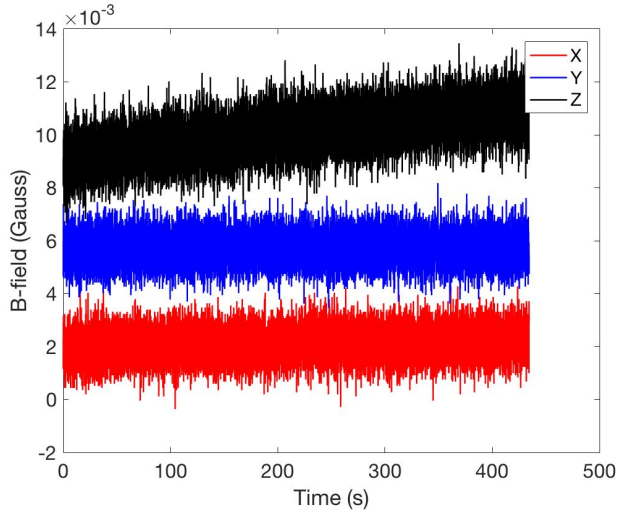


Figure 52: Pixhawk magnetometer readings from the three layer Zero Gauss Chamber lying vertically with the cap on. The drift rate of the Z-axis is noticeably more controlled in having the cap on. This data was used to calculate magnetometer drift and biases.

Five Layer Zero Gauss Chamber Test

Primary writer: Lindsay Taylor

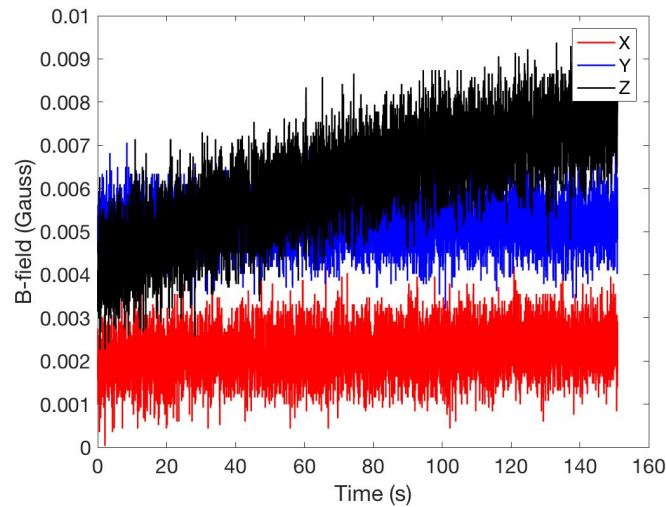


Figure 53: Pixhawk magnetometer readings from the five layer Zero Gauss Chamber lying horizontally without the cap on. The drift rate of the Z-axis magnetometer is seen greatly in this figure. This data was used to compare the effects of the 3-layer and the 5-layer Zero Gauss Chamber.

A5. Gyroscope Noise and Drift Characterization

Single Axis Changing Magnetic Field Test

Primary writer: Evan Majd

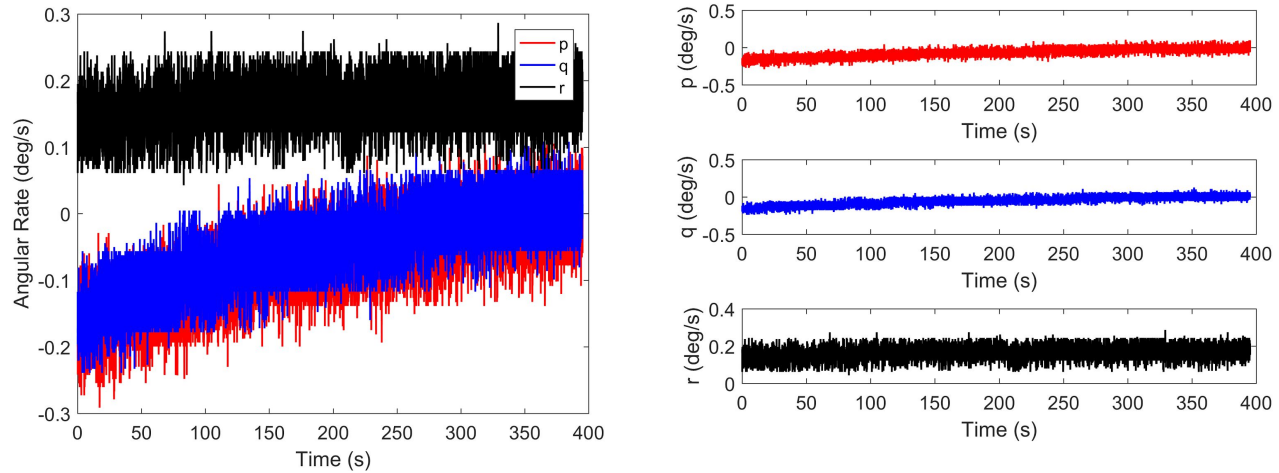


Figure 54: The magnetic field was set to 0 mG, raised up to 250 mG, decreased down to -250 mG, and then brought back to 0 mG. The rate was approximately 10 mG/s. This was run on each axis. The test starts at approximately 30 seconds where the magnetic field on all axis is set to 0 mG. Due to the axes being defined opposite for the Pixhawk and Helmholtz cage, the Pixhawk reads the X-axis and Z-axis as negative. The left plot shows the drift relative to time and the right plot shows the magnitude of noise for each axis. The drift for p, q, r are respectively $4.1484\text{e-}04$, $4.0657\text{e-}04$, and $6.3288\text{e-}05 \text{ }^{\circ}/\text{s}^2$.

Single Axis Constant Magnetic Field with Rotating Plate Orientation Test

Primary writer: Evan Majd

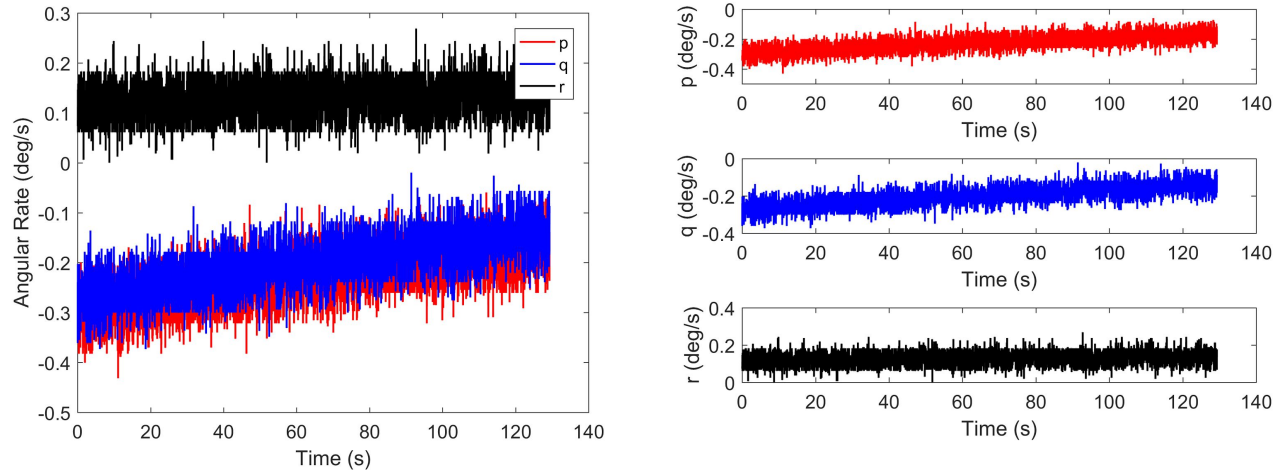


Figure 55: The magnetic field was set to 250 mG and was rotated about each axis in steps of approximately $15^{\circ}/\text{s}$. The axis of rotation was at 0 mG. The test starts at approximately 7 seconds where the magnetic field on all axes all start at zero. Due to the axes being defined opposite for the Pixhawk and Helmholtz cage, the Pixhawk reads the X-axis and Z-axis as negative. The left plot shows the drift relative to time and the right plot shows the magnitude of noise for each axis. The drift for p, q, r are respectively $1.7639\text{e-}05$, $1.8273\text{e-}05$, $2.9550\text{e-}6 \text{ }^{\circ}/\text{s}^2$.

A6. Attitude Determination Algorithm Application

X-Axis

Primary writer: Stephanie Wegner

TRIAL 1

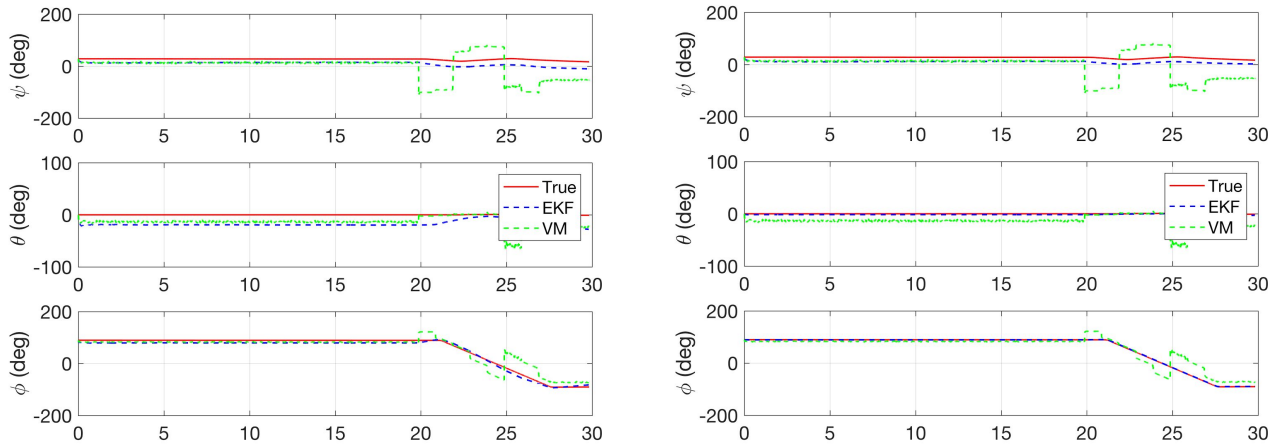


Figure 56: The magnetometer, accelerometer (“mock” sun-sensor), and gyroscope data were fed into a modified attitude determination algorithm to produce the attitude assessments described by the Extended Kalman Filter (EKF) blue lines in the above plot. This is compared to the true attitude (True) red lines, which was measured directly as Euler angles by the Pixhawk flight computer. Another method for solving attitude, vector matching (VM), is represented by green lines to show the difference between that and the EKF method for accuracy in predicting the true attitude of the system. The vector matching data is being used as the measurement update for the EKF code, which is why the EKF line looks like it represents a combination of the VM and True lines. This is directly affected by the measurement noise values contained within the EKF code for magnetometers and sun sensors (accelerometer in this case). The two plots show two different values for the magnetometer noise used in the EKF: the plot on the left uses 0.05 and the one on the right uses 0.7. It is noticeable that by inflating the magnetometer noise, the EKF lines correspond closer to the true attitude. Further analysis can be found in Section 6.1.

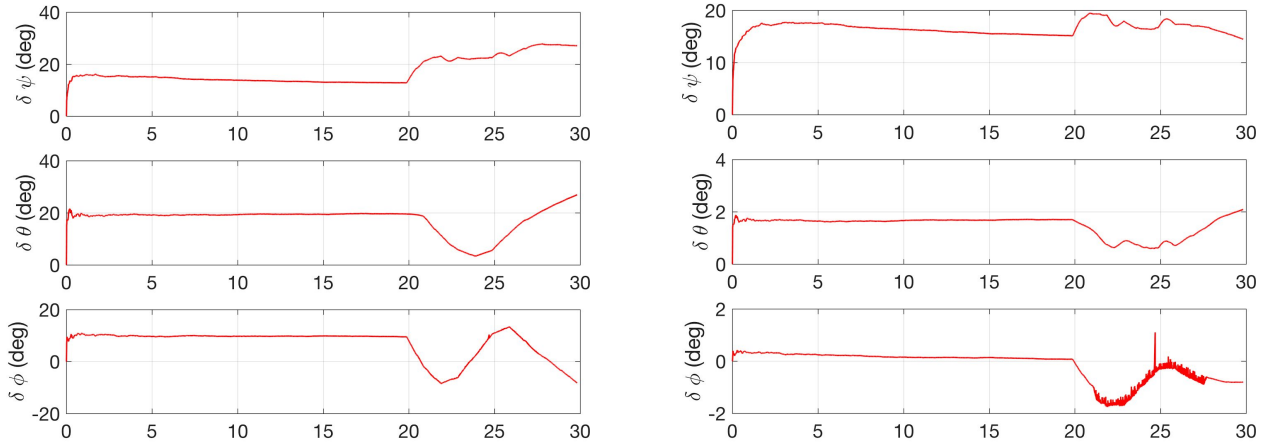


Figure 57: The magnetometer, accelerometer (“mock” sun-sensor), and gyroscope data were fed into a modified attitude determination algorithm to produce attitude assessments and compare them to the true attitude (measured directly as Euler angles by the Pixhawk flight computer). This figure shows the amount of error, in degrees, between the Extended Kalman Filter (EKF) attitude estimate and the true measured attitude. Note the difference in scale between the plots on the left and right. The error in the plot on the right is significantly less than the error in the plot on the left, at least for pitch and roll. This is due to the two plots showing two different values for the magnetometer noise used in the post-processing of the data in the attitude determination algorithm: the plot on the left uses 0.05 and the one on the right uses 0.7. It is noticeable that by inflating the magnetometer noise, the EKF lines correspond closer to the true attitude. Further analysis can be found in Section 6.1.

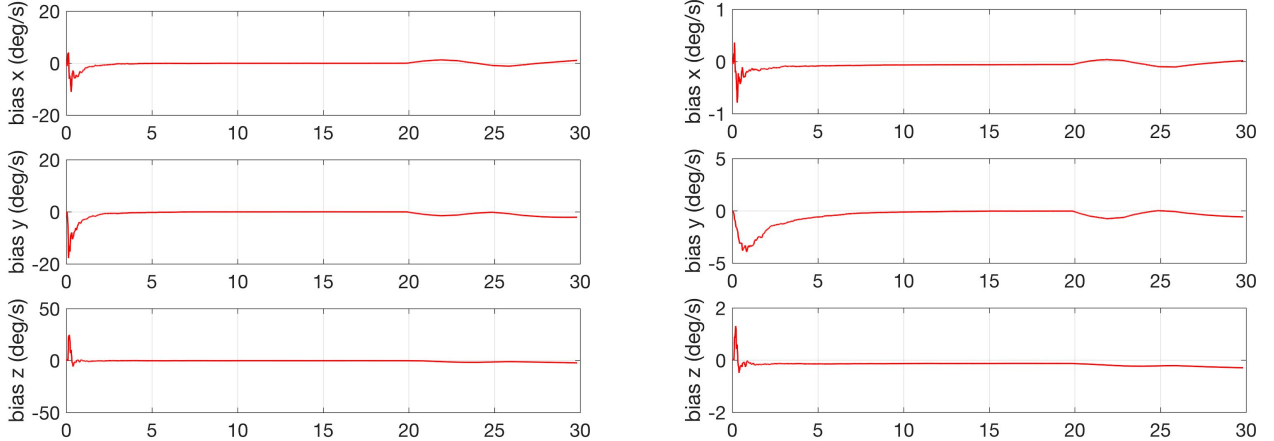


Figure 58: The magnetometer, accelerometer (“mock” sun-sensor), and gyroscope data were fed into a modified attitude determination algorithm to produce attitude assessments and compare them to the true attitude (measured directly as Euler angles by the Pixhawk flight computer). This figure shows the gyroscope bias, in degrees per second, calculated by the Extended Kalman Filter (EKF) algorithm. Note the difference in scale between the plots on the left and right. The bias in the plot on the right has significantly less variation before

settling than the bias in the plot on the left. This is due to the two plots showing two different values for the magnetometer noise used in the post-processing of the data in the attitude determination algorithm: the plot on the left uses 0.05 and the one on the right uses 0.7. It is noticeable that by inflating the magnetometer noise, the bias found in the EKF algorithm varies less. Further analysis can be found in Section 6.1.

TRIAL 2

Figures for Trial 2 are not included due to the EKF not working in the post-processing of the data. To see the figure generated of the true attitude and vector matching attitude, see the document containing X-axis figures generated from post-processing: [\[LINK\]](#). To see the accelerometer, gyroscope, and magnetometer data used to input into the EKF, see the rotating field test document containing the figures from X-axis Trial 2: [\[LINK\]](#).

TRIAL 3

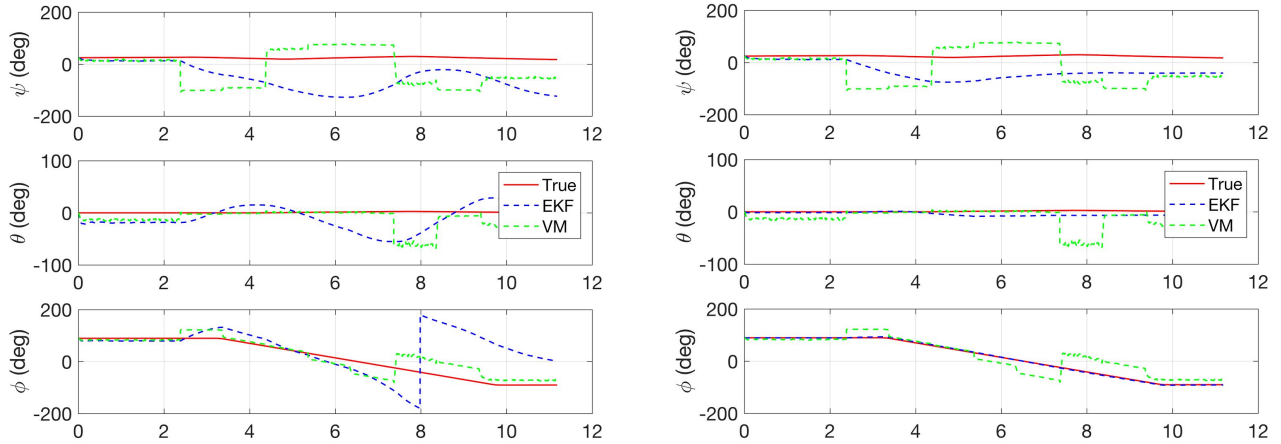


Figure 59: The Extended Kalman Filter (EKF) data is plotted with the vector matching data and true Euler angle values. The plot on the left represents a magnetometer measurement noise value of 0.05, while the plot on the right has a noise value of 0.7. It is noticeable that by inflating the magnetometer noise, the EKF lines correspond closer to the true attitude. Further analysis can be found in Section 6.1.

Note: See Figure 56 for a more in-depth description of the figure.

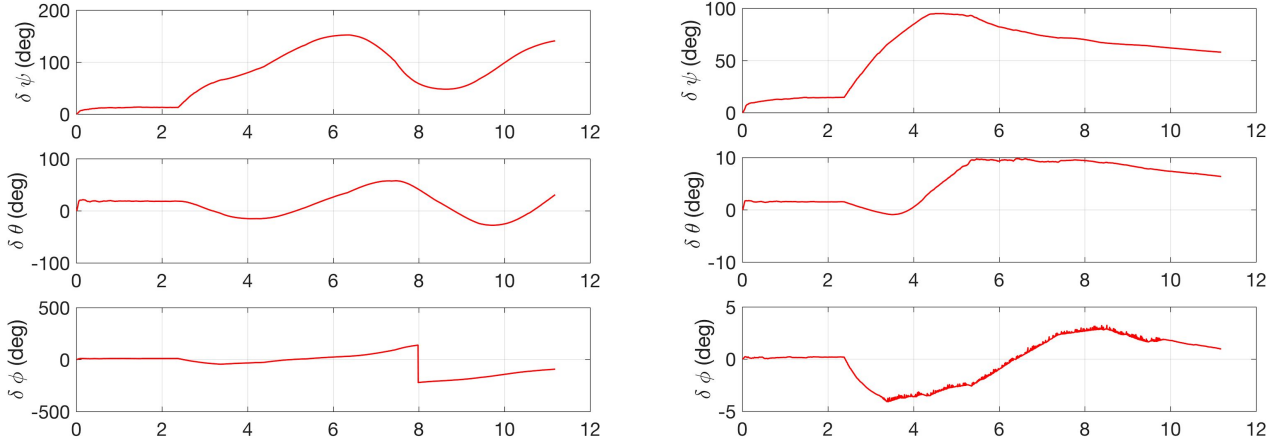


Figure 60: This figure shows the amount of error, in degrees, between the Extended Kalman Filter (EKF) attitude estimate and the true measured attitude. Note the difference in scale between the plots on the left and right. The plot on the left represents a magnetometer measurement noise value of 0.05, while the plot on the right has a noise value of 0.7. It is noticeable that by inflating the magnetometer noise, the EKF lines correspond closer to the true attitude. Further analysis can be found in Section 6.1.

Note: See Figure 57 for a more in-depth description of the figure.

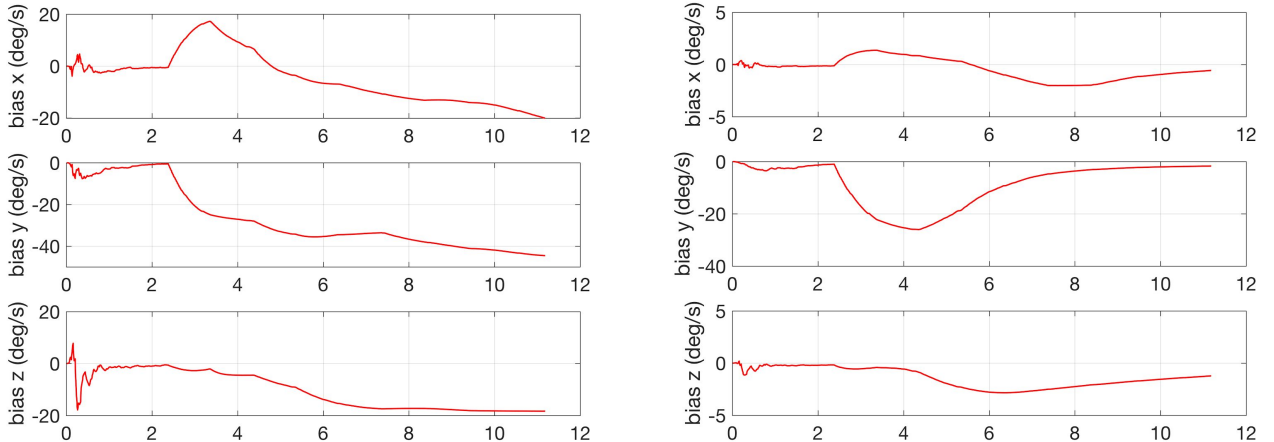


Figure 61: This figure shows the gyroscope bias, in degrees per second, calculated by the Extended Kalman Filter (EKF) algorithm. Note the difference in scale between the plots on the left and right. The bias in the plot on the right has significantly less variation before settling than the bias in the plot on the left, which does not converge at all. The plot on the left represents a magnetometer measurement noise value of 0.05, while the plot on the right has a noise value of 0.7. It is noticeable that by inflating the magnetometer noise, the bias found in the EKF algorithm varies less. Further analysis can be found in Section 6.1.

Note: See Figure 58 for a more in-depth description of the figure.

TRIAL_4

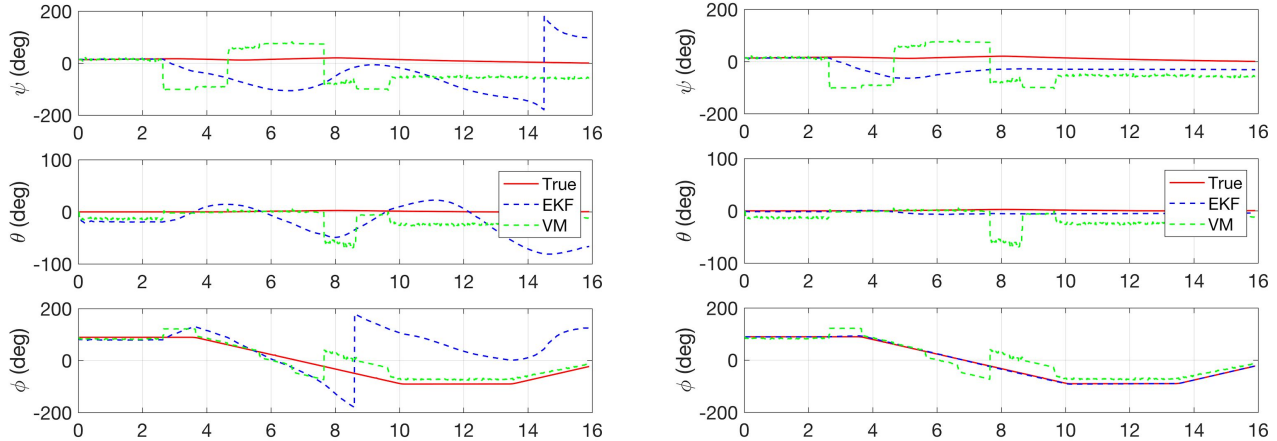


Figure 62: The Extended Kalman Filter (EKF) data is plotted with the vector matching data and true Euler angle values. The plot on the left represents a magnetometer measurement noise value of 0.05, while the plot on the right has a noise value of 0.7. It is noticeable that by inflating the magnetometer noise, the EKF lines correspond closer to the true attitude. Further analysis can be found in Section 6.1.

Note: See Figure 56 for a more in-depth description of the figure.

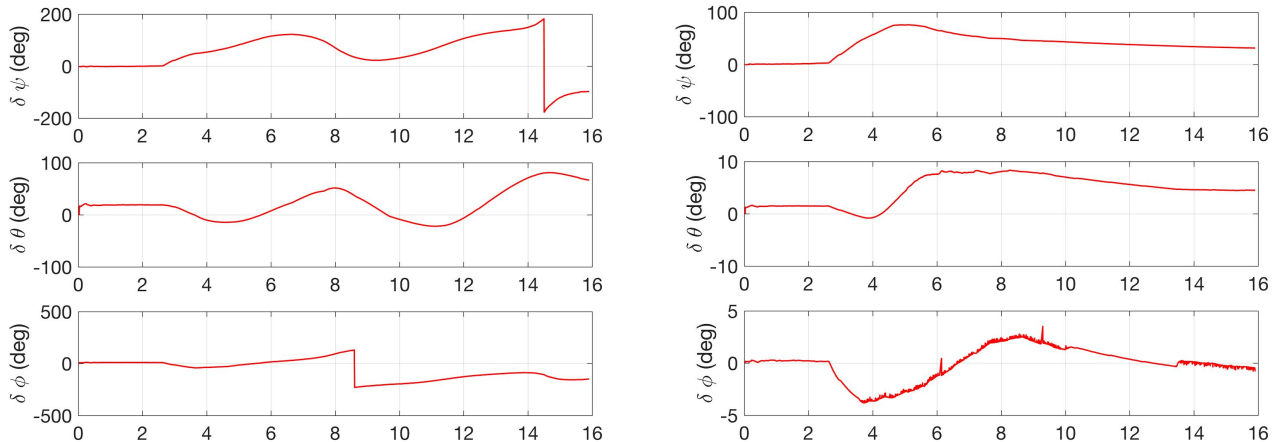


Figure 63: This figure shows the amount of error, in degrees, between the Extended Kalman Filter (EKF) attitude estimate and the true measured attitude. Note the difference in scale between the plots on the left and right. The plot on the left represents a magnetometer measurement noise value of 0.05, while the plot on the right has a noise value of 0.7. It is noticeable that by inflating the magnetometer noise, the EKF lines correspond closer to the true attitude. Further analysis can be found in Section 6.1.

Note: See Figure 57 for a more in-depth description of the figure.

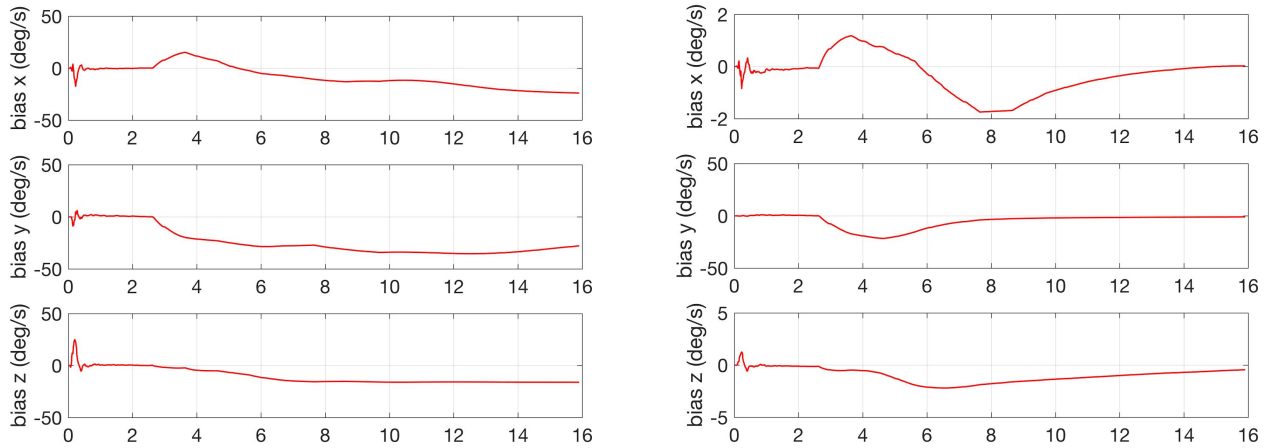


Figure 64: This figure shows the gyroscope bias, in degrees per second, calculated by the Extended Kalman Filter (EKF) algorithm. Note the difference in scale between the plots on the left and right. The bias in the plot on the right has significantly less variation before settling than the bias in the plot on the left, which also does not converge as much either. The plot on the left represents a magnetometer measurement noise value of 0.05, while the plot on the right has a noise value of 0.7. It is noticeable that by inflating the magnetometer noise, the bias found in the EKF algorithm varies less. Further analysis can be found in Section 6.1.

Note: See Figure 58 for a more in-depth description of the figure.

TRIAL 5

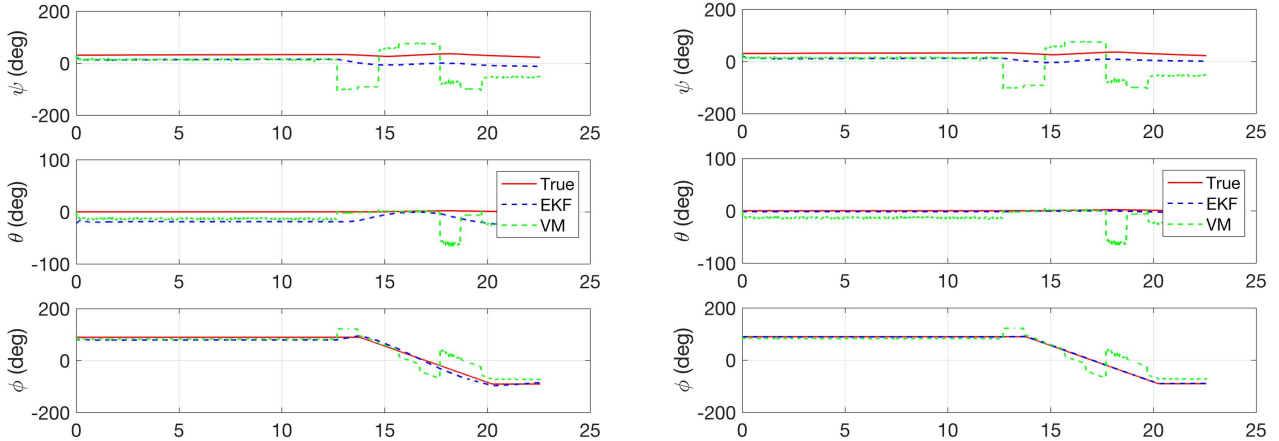


Figure 65: The Extended Kalman Filter (EKF) data is plotted with the vector matching data and true Euler angle values. The plot on the left represents a magnetometer measurement noise value of 0.05, while the plot on the right has a noise value of 0.7. It is noticeable that by inflating the magnetometer noise, the EKF lines correspond closer to the true attitude. Further analysis can be found in Section 6.1.

Note: See Figure 56 for a more in-depth description of the figure.

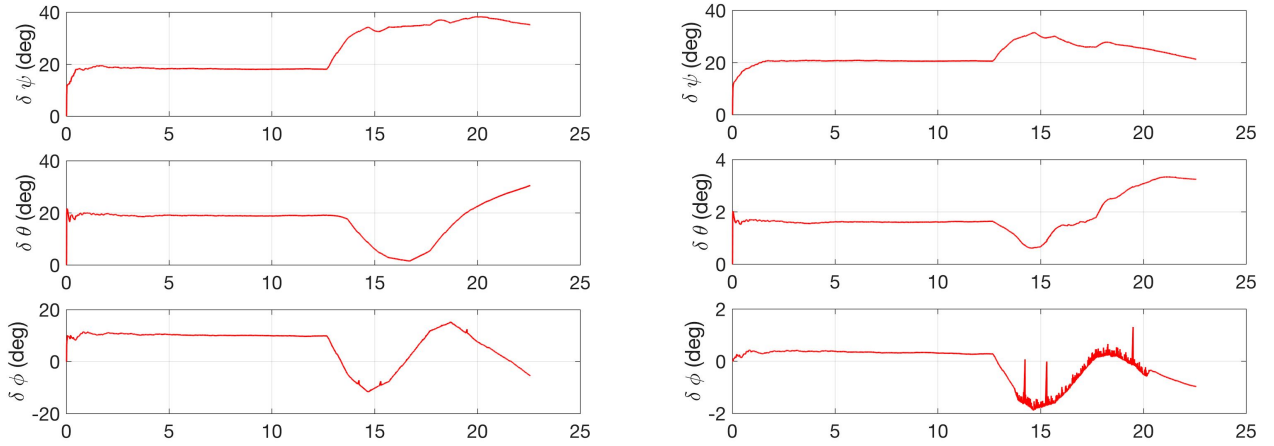


Figure 66: This figure shows the amount of error, in degrees, between the Extended Kalman Filter (EKF) attitude estimate and the true measured attitude. Note the difference in scale between the plots on the left and right. The plot on the left represents a magnetometer measurement noise value of 0.05, while the plot on the right has a noise value of 0.7. It is noticeable that by inflating the magnetometer noise, the EKF lines correspond closer to the true attitude. Further analysis can be found in Section 6.1.

Note: See Figure 57 for a more in-depth description of the figure.

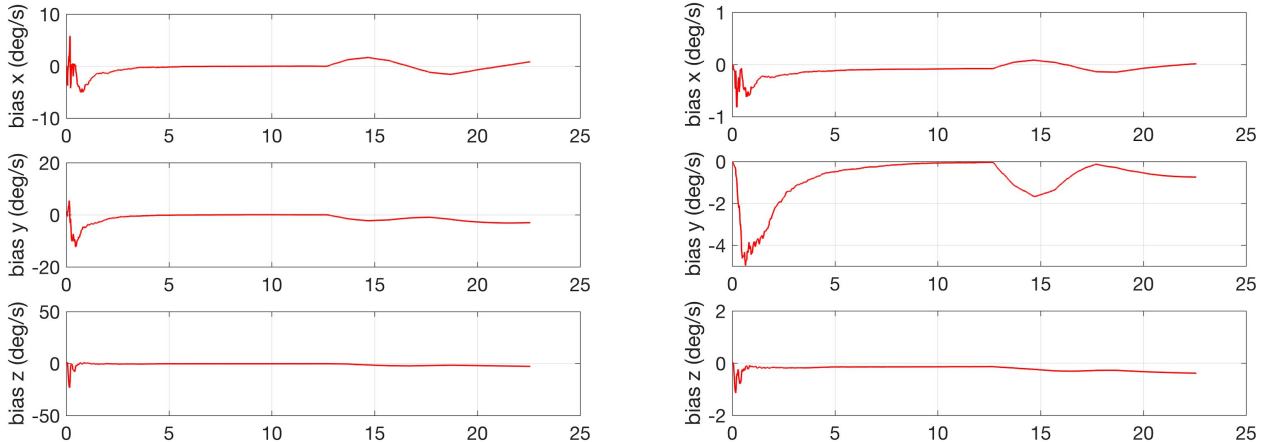


Figure 67: This figure shows the gyroscope bias, in degrees per second, calculated by the Extended Kalman Filter (EKF) algorithm. Note the difference in scale between the plots on the left and right. The bias in the plot on the right has significantly less variation before settling than the bias in the plot on the left. The plot on the left represents a magnetometer measurement noise value of 0.05, while the plot on the right has a noise value of 0.7. It is noticeable that by inflating the magnetometer noise, the bias found in the EKF algorithm varies less. Further analysis can be found in Section 6.1.

Note: See Figure 58 for a more in-depth description of the figure.

Appendix B - Atmel Development Board

Primary writer: Evan Majd

The flight computer being used is called the Atmel Development Board (AT32UC3C-3K). It is a 7" x 5.875" board and operates on the FreeRTOS operating system. It is shown below:

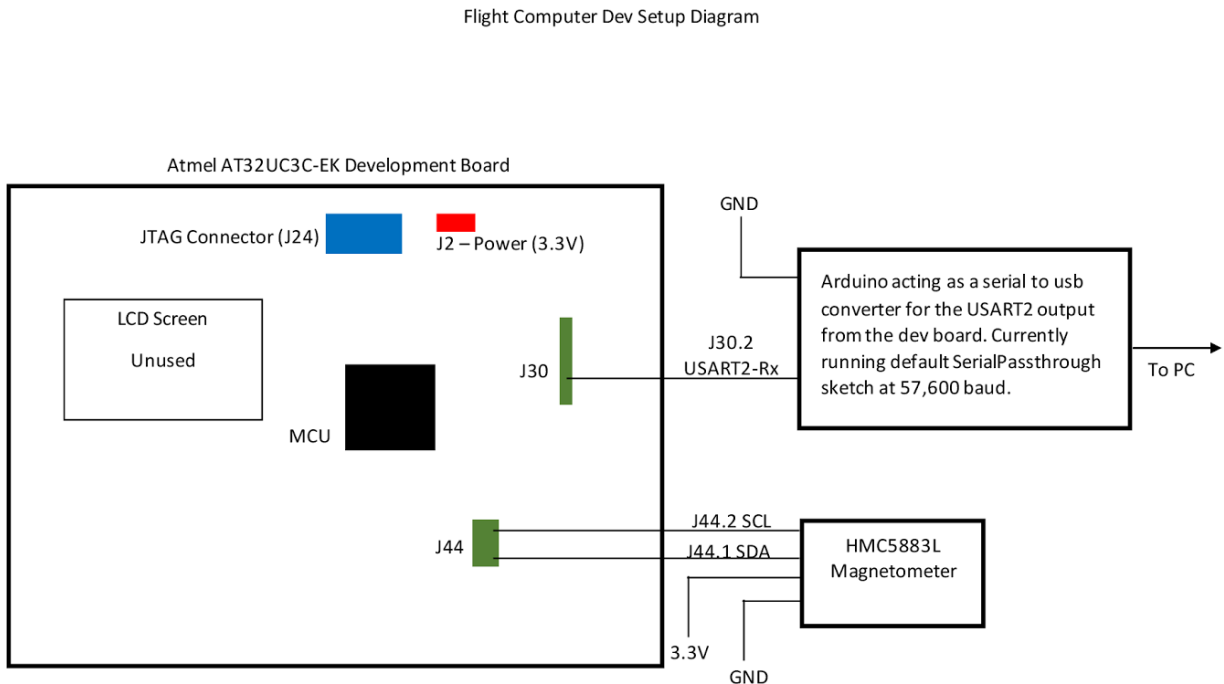


Figure 68: The brief schematic of the atmel flight computer and the locations of the necessary and important connections. The J30.2 pin connects to the Arduino, and the J44 pin connects to the magnetometer.

The Atmel is powered off the 3.3V pin on an Arduino Uno and outputs to the Arduino Uno as a serial passthrough through the J30.1 and J30.2 pins. There is one modification to the Atmel Development Board which consists of moving a resistor to an adjacent position.

The 3-axis accelerometer is built in the Atmel Development board. The 3-axis magnetometer used is the Honeywell HMC5883L. This is a .875" x .875" board that is connected to the Atmel by J44.1 and J44.2. It also requires a ground and 3.3V power supply. Both are provided by the Arduino Uno. The 3-axis gyroscope used is the Invensense MPU-3300. This is a 1.875" x 1.875" board that is connected to the Atmel by A4 and A5. It also requires a ground and 3.3V power supply. Both are provided by the Arduino Uno. All 3 sensors have tests sketches for functionality and verification.

The goal is to port the Pixhawk c-code to work with the Atmel Development Board (also c-code). This will involve minor tweaks and debugging.

Appendix C - Attitude Determination Algorithm Transfer from Matlab to C-Code

Primary writer: Evan Majd

Overview

The determination algorithm was first implemented in MATLAB to test functionality of the algorithm and verify correctness. The reason for starting with MATLAB is because C is a less user friendly environment for testing and debugging especially involving matrix manipulation. Once the code's bugs were ironed out, the algorithm was implemented in C on a disk image of a linux machine (via virtualbox) provided by Dr. Demoz Gebre. In this image, a Pixhawk environment is available to use to write C code. The C code is still being debugged and will need to be made compatible with the atmel flight computer.

MATLAB to C Conversion

The MATLAB script is divvied into 4 main parts: the solar model, the magnetic reference model, the TRIAD algorithm, and the EKF (Extended Kalman Filter) each having their respective inputs and outputs.

TRIAD Algorithm to C Conversion

The TRIAD algorithm starts off by computing the cross product between the magnetic field vector in the body frame and the solar vector in the body frame. This is done in C by using the skew operator. For example, if we want Vector_1 x Vector_2, that is equivalent to skew(Vector_1)*Vector_2. The skew function is already included in the code. Then the vector is normalized. Since this is C code, each matrix must be declared beforehand. For example the correct way to declare a 3x3 matrix is by writing Matrix<float,3,3> S; where the first part is declaring the size, and the second part 'S' gives the matrix a name. This same process is done to the magnetic field vector in the inertial frame and the sun vector in the inertial frame. Once again the same process is done to the magnetic field vector in the body frame and the magnetic field vector in the inertial frame. Once these three vectors are calculated, two rotation matrices are then made. Rotation matrix A = [m_b t2b t3b] and B = [m_i t2i t3i]. This is done in C indexing. To compute the final rotation matrix, we take A times the transpose. To find a transpose of a matrix B, it's just B.transpose(). The resulting multiplication gives the rotation matrix from inertial to body frame (3x3 matrix) which is also called a direct cosine matrix (DCM). Using the dcm2quat function, we can find the respective quaternion associated with the direction cosine matrix. If the rotation matrix is R_i_B, the quaternion is dcm2quat(R_i_B). The quaternion and rotation matrix from inertial to body frame are then returned.

EKF to C Conversion

The inputs of the EKF are the sun vector in the body frame, s_B, the magnetic field in the body frame, m_B, the sun vector in the inertial frame, s_i, the magnetic field in the inertial frame, m_i, the previous

attitude quaternion estimate, q_prev, and the previous state error covariance, P_prev. The outputs of the EKF are the attitude quaternion estimate of the satellite, q, the state error covariance, P, and the state error computed from the Kalman gain, qe.

The first section of the EKF finds the quaternion of the cubesat orientation via gyro integration. Gyro integration just takes the previous cubesat orientation quaternion and adds the change in quaternion over a small timestep. This is done by first initializing then assigning values to a 4x4 matrix B. The assignment of values is done via indexing. A fast way to input data into a matrix in C is to make an array then assign the array values to a matrix. For example, If you have a 4x4 matrix, then there will need to be 16 values. The first four values will be assigned to the first row, second four to the second row and so on. This is done with the following two lines,

```
float B_data[16] = {input values here separated by spaces};
Matrix<float,4,4> B(B_data);
```

Then the change in quaternion can be calculated by taking the transpose of B*q_prev and divided that by 2. I found it easier to multiply by .5 rather than divide by two to avoid errors. The quaternion is then normalized using the quatnormalize() function and is now the updated quaternion vector for the cubesat orientation.

The second section is to propagate the state covariance. We first want to create the inputs F, G, dt, and Rw. This had to be implemented a little differently in C since the functions used in MATLAB are exclusive to MATLAB. First an identity matrix is created. This is done by the following two lines,

```
Matrix<float,3,3> I;
I.setIdentity();
```

The setIdentity() operator just sets all diagonal components of the matrix to 1, and the rest to 0. The G matrix is then just created by multiplying the identity matrix by -.5 (or dividing by -2). The gyro bias is .005 deg/s. This is converted to radians by multiplying by d2r, squared, and then multiplied by the identity matrix to get the Rw matrix. To square a value, the pow() function is used as so,

```
pow(.005*d2r,2);
```

The F matrix just consists of gyro sensor values and is indexed using the method described above. Dt is previously defined to be .1. The disrw C function is an approximation of the disrw function in matlab. This function is computationally expensive which is why I went with the approximation. It can be found at <http://www.gnssapplications.org/chapter7.html> being the first download link. Inside this folder the file is called discrete_processing_noise.m. I will also include the code for it in this documentation. The approximation uses the equation

$$Q_k = (I + dt * F) * (dt * G * R_w * G.transpose())$$

Where Q_k is the value we want returned (is Cd in the code). The state error covariance, P, is then calculated using the lines,

```
PHI = I+F*.1;
P = PHI*P_prev*PHI.transpose() + Cd;
```

The third section is used to calculate the z, H, and Rz values. The magnetic field vector and sun vector in the body frame estimates are set to a zero vector first. The rotation matrix from navigation to body frame is then created (3x3 matrix) which is called C_n2b and is set to the identity matrix as previously described. The MATLAB script uses inherent MATLAB functions quatrotate and quat2dcm to do the next few calculation. I have not gotten the quatrotate function to work for C yet. To find m_b_est and s_b_est we want to rotate the gyro quaternion vector about the magnetic field inertial vector (m_i) and sun inertial vector (s_i). Once those are calculated the z and H matrices can be made via indexing. The DCM matrix is then calculated by using a similar method explained. The resolution matrices for the magnetometer and sun vector are now made. For the magnetometer $R_m = I^{*.02}$ and for the sun sensor $R_s = I^{*.05}$. Since C has no easy way to index matrices, I spent the next few lines assigning the previously calculated vectors to the Rz matrix (6x6) via indexing.

The fourth section of the code is used to compute the kalman gain and update the quaternion vector. The first matrix L, is a 3x6 matrix calculated via,

```
L = P*H.transpose()*pow(H*P*H.transpose())+Rz,-1);
```

The second matrix q_e, is a 3x1 matrix calculated via,

```
q_e = L*z;
```

The qe matrix is a 1x4 matrix made by indexing the q_e matrix values. The updated quaternion now is calculated with,

```
q = qgyro*qe;
```

and normalized by,

```
q.normalize();
```

The last part of the code is used to update the state error covariance with all the values we have previously calculated. This is done by,

```
P = (I-L*H)*P;
```

The values returned are the updated quaternion, q, the quaternion state error, qe, and the update state error covariance matrix P.

Solar Model

The section of code still needs to be finished. It consists of two parts. Finding the julian date of a specified UTC and using that to find the sun vector. The other part converts the latitude, longitude, and altitude data to a more use form called ECI (earth centered inertial coordinate frame). Julian date can be calculated with a given UTC using the following formula.

$$T_{JD} = K - 32075 + 1461 * (I + 4800 + (J - 14) / 12) / 4 + 367 * (J - 2 - (J - 14) / 12 * 12) * 2 / 12 - 3 * ((I + 4900 + (J - 14) / 12) / 100) / 4;$$

The part where you get the sun vector is still a part being worked on. I suggest reaching out to a professor who knows this well. Otherwise Prof. Gebre told us to use the gravity vector as a placeholder to get the algorithm up and running. This vector should be in km.

For the lla to ECI conversion that is also still being worked on. IT has to be broken up into two parts converting lla to ecef (earth centered earth fixed frame) then converted from ecef to eci. The lla2ecef part is done with simple equations. I would suggest once again talking to a professor to find the conversion code for ecef to eci because I was not able to find it or figure it out. Once the ECI coordinates are figured out, they will be in meters and will need to be converted to km which is done with the line,

$$\text{Pos_eci_km} = \text{pos_eci_m} * .001;$$

To get the sun vector, the position vector of the cubesat and the sun vector are subtracted from each other and then normalized. The sun vector, s_ECI is then returned.

Magnetic Reference Model

The code for the magnetic reference model has not yet been produced. The code should be able to able to find the magnetic field in ECI frame given lla and time. I have had trouble finding a model in C. Once again, I suggest talking to a professor to figure this out.

Testing and Compiling

The code was compiled in the linux image Prof. Gebre provided us. Using a special script called umn_algorithm.m, one can drop their code inside this boolean update function and test for compiling errors and test values by printing them off to screen or saving them to a csv file.

Future Work

The code needs to be further tested and debugged. The values need to be compared to MATLAB outputted values to make sure it is calculating the correct values. The Solar and magnetic reference models need to be finished. Once all of this is done, the code needs to be ported to the atmel flight computer.

The code can be found in CubeSat Senior Design > PIX HAWK IMAGE, PDFs, Code
https://drive.google.com/drive/folders/0B03IGxMuEuw_N1NMVVJoUks0amM

References

1. Brewer, Megan R. "Cubesat Attitude Determination and Helmholtz Cage Design." 2012. Air Force Institute of Technology.
2. Products, Sensor. "Cross Axis Effect for AMR Magnetic Sensors." *Honeywell Sensor Products* (n.d.): n. pag. Honeywell. Web.
https://aerocontent.honeywell.com/aero/common/documents/myaerospacecatalog-documents/Defense_Brochures-documents/Magnetic__Literature_Application_notes-documents/AN215_Cross_Axis_Effect_for_AMR_Magnetic_Sensors.pdf.

Acknowledgements

Thank you to Honeywell for use of their facility and hospitality during testing. Specifically Mike Freeman for assisting us on each day of testing with the Helmholtz cage and Zero Gauss Chamber. We would also like to thank Tracy Sellin, Kim Class, Dianne Ekhaml, Bharat Pant, Donnette Peterson, and Kory Robeck for their assistance.

Thank you to Professor Demoz Gebre for providing advice and guidance, and being a knowledgeable resource for our system and testing procedures.

Thank you to our senior design course professors, John Weyrauch and Bill Garrard, for providing guidance and advice throughout the year on both technical and non-technical aspects of our project.